Macdonald, F.M., Swanson-Hysell, N.L., Park, Y., Lisiecki, L., and Jagoutz, O. (2019), Arc-continent collisions in the tropics set Earth's climate state *Science* doi:10.1126/science.aav5300

Arc-continent collisions in the tropics set Earth's climate state

Authors: Francis A. Macdonald[1]*, Nicholas L. Swanson-Hysell[2], Yuem Park[2], Lorraine Lisiecki[1], Oliver Jagoutz[3]

Affiliations:

[1]Department of Earth Science, University of California, Santa Barbara, CA 93106

[2]Department of Earth and Planetary Science, University of California, Berkeley, CA 94720

[3]Department of Earth, Atmospheric, and Planetary Sciences, Massachusetts Institute of Technology, Cambridge, MA 02139

*Correspondence to: francism@ucsb.edu

Abstract: On multi-million-year timescales, Earth has experienced warm ice-free and cold glacial climates, but it is unknown if transitions between these background climate states were the result of changes in CO_2 sources or sinks. Low-latitude arc-continent collisions are hypothesized to drive cooling by uplifting and eroding mafic and ultramafic rocks in the warm, wet tropics, thereby increasing Earth's potential to sequester carbon through chemical weathering. To better constrain global weatherability through time, the paleogeographic position of all major Phanerozoic arc-continent collisions was reconstructed and compared to the latitudinal distribution of ice-sheets. This analysis reveals a strong correlation between the extent of glaciation and arc-continent collisions in the tropics. Earth's climate state is set primarily by global weatherability, which changes with the latitudinal distribution of arc-continent collisions.

One Sentence Summary: Through the Phanerozoic Eon, glacial climates occur during intervals of extensive arc-continent collision in the tropics.

Main Text: Over geological history, Earth's climate has varied between warm ice-free climate states, and cold glacial climate states in which polar continents were covered in ice (*1*, *2*). Through the Phanerozoic Eon (past 540 Myr), Earth's climate has been predominantly non-glacial (~75%), with relatively brief, ~3-60 Myr intervals of glacial climate (*1*, *3*). Similarly, aside from Snowball Earth events, much of the preceding Proterozoic Eon was also characterized by a non-glacial climate state (*3*). Given that a warm, non-glacial climate is the most common climate state for Earth, what processes have caused cooling trends on million-year timescales resulting in glacial climate states, like observed today?

Earth's climate state is set by the balance between geological sources and sinks of carbon to the ocean-atmosphere system, but their relative importance is uncertain (*4*-*8*). On long time-scales, CO_2 is emitted by volcanism and consumed by chemical weathering of silicate rocks, which delivers alkalinity through rivers to the ocean and sequesters carbon via the precipitation of carbonate rocks. Prolonged imbalances between the magnitude of the sources and sinks would catastrophically manifest in either the onset of a Snowball Earth or a runaway greenhouse (*7*). The relative clemency of Phanerozoic climate requires that CO_2 sinks scale with changes in the sources, which can be explained through the silicate weathering feedback where elevated CO_2 leads to

higher temperatures and invigorated hydrological cycling that enhances chemical weathering and vice versa (*4*). Because of the silicate weathering feedback, a decrease in the CO_2 flux to the atmosphere leads to decreased weathering until a new steady state is achieved at lower CO_2 concentrations in the atmosphere (*4, 7*). CO_2 levels also vary due to changes in global weatherability — the cumulative factors that affect chemical weathering aside from climate (*8*). Global weatherability is the product of variables such as lithology, topography, and paleolatitude (*8, 9*). An increase in global weatherability also results in cooling as the consumption of carbon through silicate weathering will match that of volcanic input at lower concentrations of atmospheric CO_2.

Present day global CO_2-consumption estimates emphasize the importance of highly weatherable areas: ~10-20% of land area is responsible for ~50-75% of CO_2 consumption through silicate weathering (*10, 11*). These highly weatherable areas, e.g. Southeast Asia, are mainly situated in the warm, wet tropics with significant topographic relief, and are composed of Ca- and Mg-rich mafic and ultramafic rocks, which have faster dissolution rates than felsic rocks (*8-12*). In general, basaltic watersheds in the tropical rain belt have about two orders of magnitude higher CO_2 consumption rates than granitic watersheds outside of the tropics (*13*).

In modern climate, the annual migration of the intertropical convergence zone results in a tropical rain belt within 10-20º of the equator (Fig. S5). The tropical rain belt is below the ascending branch of the Hadley circulation, which has been confined to low-latitude throughout Earth History (*14*). Thus, geological data coupled with paleogeographic reconstructions can be used to estimate changes in topography and lithology within the tropical rain belt through time. Importantly, as climate warms or cools, the tropics remain relatively warm and wet with high weathering rates such that global weatherability is particularly sensitive to paleogeographic changes in the tropics (*15-17*).

Phanerozoic cooling trends have been previously attributed to a decrease in CO_2 output from volcanism (*6, 18*), or an increase in global weatherability through mountain building (*2, 5, 8*) or the drift of mafic rocks associated with large igneous provinces (LIPs) through the tropics (*15*). Recently, it was proposed that low-latitude arc-continent collisions combine these processes by terminating subduction related volcanic CO_2 outgassing along the collided segment, while also increasing global weatherability by actively uplifting volcanic arcs in the warm, wet tropics (*19*).

During arc-continent collisions volcanic arcs are obducted onto continents creating ophiolites, which are preserved along suture zones and mark the position of former oceans. Arcs and ophiolites are composed predominantly of basalt and ultramafic rocks that are Ca- and Mg-rich and effective at consuming CO_2 through silicate weathering (*8-13, 20*). Ophiolites in collisional belts can extend tens of thousands of kilometers along strike and be progressively exhumed as they are thrust over a continental margin. The combination of high chemical weathering rates in the tropics and the generation of topography during exhumation makes low-latitude arc-continent collisions particularly effective at liberating the large quantities of cations in arcs to the ocean, thereby increasing global weatherability and driving global cooling (*19*).

The process of arc-continent collision in the tropics has been invoked to explain specific cooling episodes during the Ordovician and Late Cretaceous to Oligocene (*19, 21*), but are intervals of extensive tropical suture length uniquely associated with intervals of cool climate? To test this hypothesis, we created a database of Phanerozoic ophiolite-bearing sutures associated with arc-continent collisions that we reconstructed with paleogeographic models (*22*). These geological

reconstructions (Fig. 1, S1; Movie S1) provide a framework for analyzing the relationships between the latitudinal distribution of highly weatherable lithologies and Phanerozoic climate change. Particularly, we compare the length of active sutures in the tropics through time with the Phanerozoic record of glaciation (Figs. 2, S2). Ophiolite obduction along a suture was deemed active from the time of the first evidence of arc exhumation, such as the appearance of ophiolite detritus in the foreland, to the age of the final collision, preferably defined by the cessation of foreland deposition.

Our results show that global active suture zone length varied significantly through the Phanerozoic between 0-30,000 km. Peaks in total suture length (between 10,000-30,000 km) are associated with major tectonic events such as the Taconic (~465-440 Ma), early Uralian (~375-358 Ma), Hercynian (~340-300 Ma), Central Asian (~250-220 Ma), Himalayan (~50-0 Ma), and Indonesian (~20-0 Ma) orogenies (Fig. 2A). Some of these orogenic events resulted in significant ophiolite obduction within the tropics (Fig. 2B) as these collisions occurred at low-latitude in roughly east-west oriented orogenic belts. Because of their geometry, the Taconic, Hercynian, Himalayan, and Indonesian orogenies had 5000-15,000 km long sutures that were within 15° of the equator. In contrast, the early Uralian and Central Asian orogenies, occurred at mid- to high-latitudes with less than 3000 km suture length exposed in the tropics (Fig 2B).

To characterize Earth's climate state through the Phanerozoic, we use the latitudinal extent of continental ice-sheets, which were compiled with updated age constraints (Fig. 2C; Table S3). While extent of glaciation is an imperfect proxy for global climate, Phanerozoic pCO_2 estimates are very uncertain (*24*). Over the Phanerozoic there have been three major glacial intervals, in the Late Ordovician (~455-440 Ma), Permo-Carboniferous (~335-280 Ma), and the Cenozoic (~35-0 Ma), with a smaller glacial advance in the Late Devonian (~360 Ma). Similarly, the major peaks in the record of suture length in the tropics are in the Late Ordovician, the Permian-Carboniferous, and the Cenozoic (Fig. 2B). Importantly, there are not major tropical suture length peaks during extended periods of non-glacial climate (e.g. the Mesozoic; 250-65 Ma).

To provide a statistical test of the correlation between arc-continent collisions in the tropics and glaciation, we evaluated whether suture length (*22*) correlates better with the real ice extent record than with randomly generated synthetic records of ice extent (i.e., simulating the null hypothesis that ice extent is independent of the proposed forcing). Synthetic ice extent records with 5 Myr resolution were generated by randomly varying the timing of four glacial episodes (Late Ordovician, Late Devonian, Permo-Carboniferous, and Cenozoic) over the past 520 Myr (Fig. S6). We also compared the percent of overlap between records, i.e. time steps containing both glaciation and significant suture length (Fig. S7). This analysis reveals that ice extent correlates strongly with tropical ($r=0.66$-0.59) and total ($r=0.57$) suture length, with statistical significance relative to the null-hypothesis ($p<0.01$), and that ice extent lacks correlation with high-latitude sutures ($r=-0.06$, $p=0.55$) (Fig. S8; Table S4). The strongest correlation is between ice extent and sutures <20º of latitude ($r=0.66$), where under the null hypothesis, only 0.002% of the random simulations of ice extent correlate as well as the observed data (Table S4); results are similar for sutures within 15º of the equator. Correlations were found to be relatively insensitive to age uncertainties when age errors in aggregate suture length were simulated using a random walk scaled to a maximum of 5 or 10 Myr (Fig. S8).

The peaks in suture length within the tropics that correspond with the three major glacial intervals are each ~10,000 km. This is approximately the length of present-day sutures in the tropics in the Indonesian orogenic system including New Guinea and the Philippines. Currently,

this region, which includes two of the three largest ophiolites on Earth (*25*), is estimated to account for ~9-14% of the modern global carbon sink (*10, 11*). We propose that the increasing exhumation of the ophiolite-bearing sutures in Indonesia and New Guinea has been a major factor in Middle Miocene to present cooling by increasing global weatherability.

From the present maximum in suture length in the tropics, there is a local minimum in active sutures at ~25 Ma (Fig. 2B). This minimum broadly coincides with the Late Oligocene to Middle Miocene warm interval. A second Cenozoic peak in suture length in the tropics occurs during the Eocene leading up to the initiation of Antarctic glaciation. The two-pronged cooling trend from the Late Cretaceous to Eocene (*26*) has been attributed to low-latitude arc-continent collision (*19*) and corresponds with local maxima in suture length in the tropics (Fig. 2B).

The Permo-Carboniferous glaciations have classically been related to an increase in carbon storage on land (*27*). Recently, it was proposed that the low-latitude Hercynian orogeny was sufficient to initiate glaciation (*17*). Our data broadly support the later hypothesis, but highlight the importance of a specific phase of mountain building, that is, the exhumation of ophiolites in the tropics. Our results also confirm that Late Ordovician glaciation was coincident with low-latitude arc-continent collision in the Taconic orogeny (*21*), Kazakh terranes, Tarim and North China (*28*).

Like the Eocene, the Early Ordovician increase in suture length in the tropics precedes glaciation by ~10 Myr. This lag may be due to warm background climate states and low global weatherability during the early Cenozoic and early Paleozoic, such that significant and prolonged increases in global weatherability were necessary to drive cooling and initiate glaciation. Indeed, oxygen isotope records from both the Eocene and Ordovician demonstrate long-term cooling trends prior to glaciation (*21*, *26*).

The Cenozoic seawater rise in radiogenic Sr and Os isotopes appears inconsistent with our hypothesis, as arcs contain relatively unradiogenic Sr and Os. However, these trends can be attributed to the differential uplift of Great and Lesser Himalayan lithologies (*29*). That isotopically unique source rocks can drive seawater Sr and Os isotope records complicates their use as a global radiogenic to juvenile weathering proxy.

The hypothesis evaluated here, that the Earth's climate state is set by the presence or absence of arc-continent collisions in the tropics, is analogous to proposals that have linked the drift of LIPs into the tropics as a driver for Cenozoic (*15*) and Neoproterozoic cooling (*16*). We have performed a similar analysis of the paleolatitude of LIPs through time (Figs. S3, S4), in which we imposed two post-emplacement scenarios, one with exponential decay of LIP areas with a 100 Myr half-life, and a second in which there is also burial of LIPs associated with rifting and subsidence (*22*). In both scenarios, area of total LIPs at all latitudes and LIPs above and below 15º have a negative to zero correlation with ice extent, with the exception of the decay plus burial scenario at <15º, which has a weakly positive correlation coefficient of r=0.10 (Fig. S9; Table S4). The lack of a clear relationship between LIP area and climate state (Fig. S4) may be due to regolith development and soil shielding in the absence of active uplift (*10*). In contrast, arc-continent collisions create active topography limiting the effect of shielding and facilitating high local weathering rates.

Because arc-continent collisions terminate subduction-related volcanism along the collided segment, cooling may also be due to reduced volcanic activity and CO_2 output (*19*). However, the high total suture length related to the Central Asian and the early Uralian orogenies during non-

glacial intervals demonstrate that reduction in arc length and volcanic CO_2 output alone are not sufficient to push the global climate into a glacial climate state. These results indicate that changes in chemical weatherability due to low latitude arc-continent collision and associated ophiolite obduction are the primary driver of global cooling trends and reduction in volcanic CO_2 output is of secondary importance.

Alternatively, it has been proposed that the extent of continental arc-volcanism is responsible for long-term climate change (*18, 30*). To quantify the strength of this proposed correlation, Phanerozoic ice extent was compared to a compilation of continental arc length (*30*). A Mesozoic peak and Cenozoic low in continental arc length results in a significantly weaker correlation with arc length (r=0.38) than that for the suture records ($<15^o$ r=0.64, $<20^o$ r=0.66) (Fig. S9; Table S4).

While we acknowledge that volcanic outgassing must have changed through time, and that organic carbon burial also had an impact on long-term climate, our analysis suggests that global weatherability has provided the first-order control on Earth's climate state. Particularly, arc-continent collisions in the tropics, such as the Indonesian orogenic system today, are ephemeral on geological timescales, and when they drift out of the tropics or exhumation ceases and topography is eroded away, the Earth returns to a non-glacial climate state. Thus, our model accounts for both the initiation and termination of ice ages. This pattern has repeated at least three times throughout the Phanerozoic — when there have been abundant tracts ophiolites being exhumed and eroded in the tropics the Earth has been in a glacial climate state, and when not, the Earth has been in a non-glacial climate state.

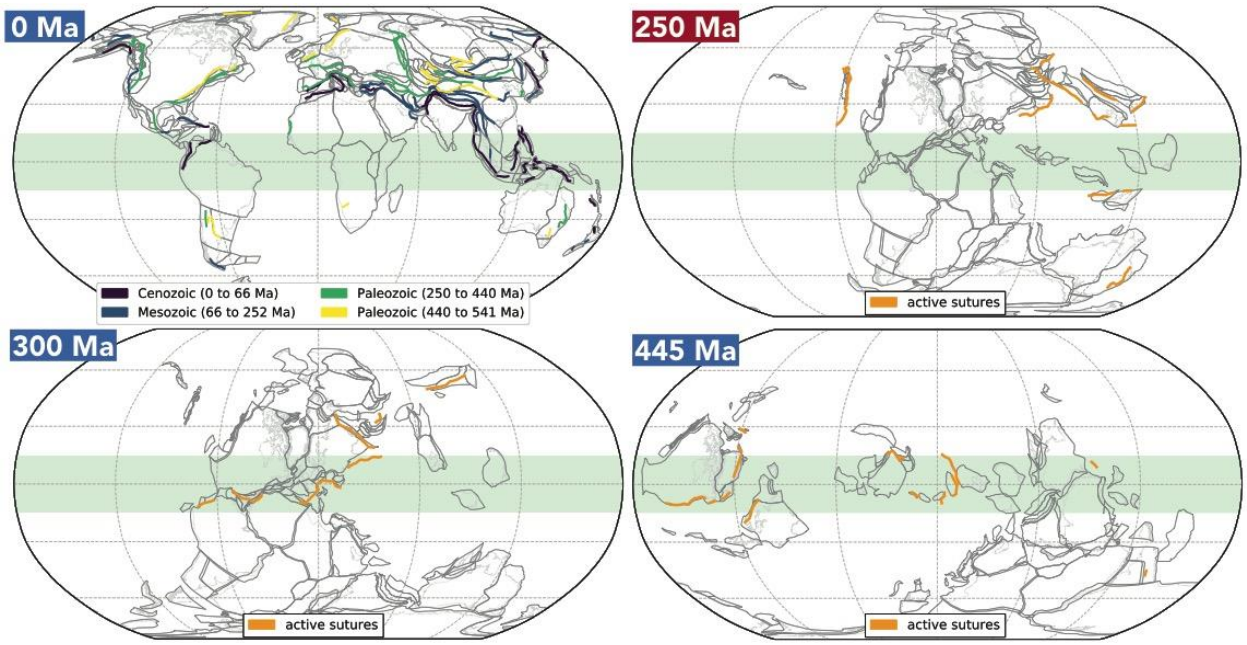

Fig. 1. Reconstructions of ophiolite-bearing sutures. All sutures within the compilation are shown in present-day coordinates in the 0 Ma map and are color-coded by age. The tropical rain belt is shaded green. Continental outlines shown are tectonic units of Torsvik and Cocks (*23*). Paleogeographic reconstructions of these tectonic units and actively exhuming sutures are shown at the times of peaks in total suture length (Fig. 2). The Triassic (250 Ma) peak in total suture length is at a non-glacial interval (red) with minimal suture length in the tropics. The Carboniferous (300 Ma) and Ordovician (445 Ma) peaks are both during glacial intervals (blue) and have significant suture length in the tropics.

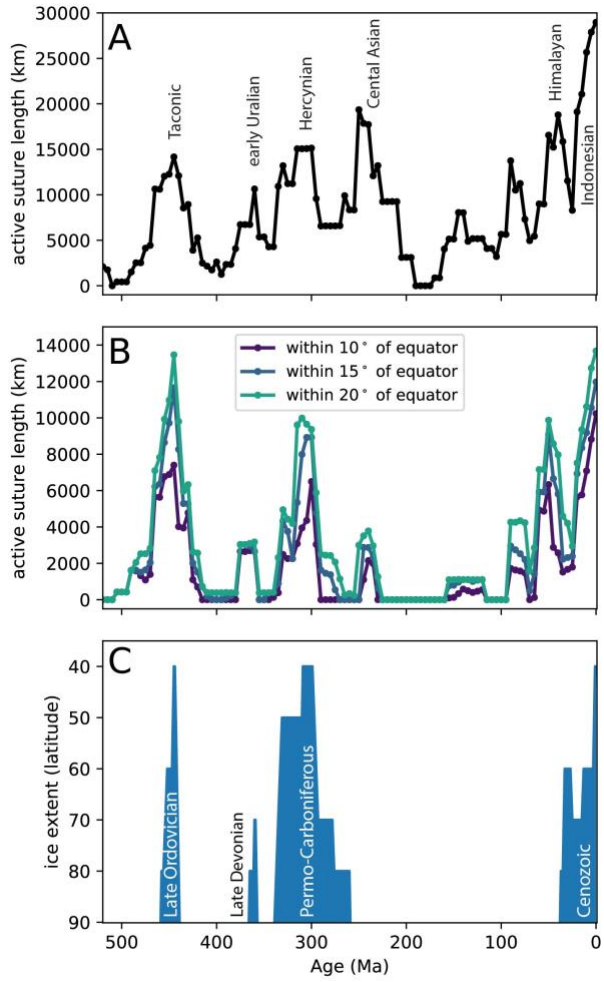

Fig. 2. Phanerozoic suture length in the tropics compared to the latitudinal extent of continental glaciation. A) Total length of active suture length. B) Total length of active sutures that are reconstructed to be within 10°, 15°, and 20° of the equator over the past 520 million years. C) Blue marks the latitudinal extent of continental ice sheets, excluding Alpine glaciers (Table S3).

References and Notes:

1. C. E. P. Brooks, *Climate Through the Ages. A Study of the Climate Factors and Their Variations*. (R.V. Coleman, New York, 1926).
2. T. C. Chamberlin, *The Journal of Geology* **7**, 545-584 (1899).
3. P. F. Hoffman, *Geology Today* **25**, 100-107 (2009).
4. J. C. G. Walker, P. B. Hays, J. F. Kasting, *Geophysical Research Letters* **86**, 9776-9782 (1981).
5. M. E. Raymo, *Geology* **19**, 344-347 (1991).
6. R. A. Berner, *American Journal of Science* **294**, 56-91 (1994).
7. R. A. Berner, K. Caldeira, *Geology* **25**, 955-956 (1997).
8. L. R. Kump, M. A. Arthur, in *Tectonic Uplift and Climate Change*. (Springer, 1997), pp. 399-426.
9. J. Gaillardet, B. Dupré, P. Louvat, C. Allegre, *Chemical Geology* **159**, 3-30 (1999).
10. J. Hartmann, N. Moosdorf, R. Lauerwald, M. Hinderer, A. J. West, *Chemical Geology* **363**, 145-163 (2014).
11. C. Dessert, B. Dupré, J. Gaillardet, L. M. François, C. J. Allegre, *Chemical Geology* **202**, 257-273 (2003).
12. K. Lackner, C. Wendt, D. Butt, E. Joyce Jr., D. Sharp, **20**, 1153-1170 (1995).
13. C. Dessert *et al.*, *Earth and Planetary Science Letters* **188**, 459-474 (2001).
14. D. A. Evans, *Nature* **444**, 51-55 (2006).
15. D. V. Kent, G. Muttoni, *Climate of the Past* **9**, 525 (2013).
16. Y. Godderis *et al.*, *Earth and Planetary Science Letters* **6648**, 1-12 (2003).
17. Y. Goddéris *et al.*, *Nature Geoscience* **10**, 382 (2017).
18. N. R. McKenzie *et al.*, *Science* **352**, 444-447 (2016).
19. O. Jagoutz, F. A. Macdonald, L. Royden, *Proceedings of the National Academy of Sciences* **113**, 4935-4940 (2016).
20. H. Schopka, L. Derry, C. Arcilla, *Geochimica et Cosmochimica Acta* **75**, 978-1002 (2011).
21. N. L. Swanson-Hysell, F. A. Macdonald, *Geology*, G38985. 38981 (2017).
22. See Online Supporting Material.
23. T. H. Torsvik, L. R. M. Cocks, *Earth History and Palaeogeography*. (Cambridge University Press, 2017).
24. G. L. Foster, D. L. Royer, D. J. Lunt, *Nature Communications* **8**, 14845 (2017).
25. C. Monnier, J. Girardeau, R. C. Maury, J. Cotten, *Geology* **23**, 851-854 (1995).
26. B. Cramer, K. Miller, P. Barrett, J. Wright, *Journal of Geophysical Research: Oceans* **116**, (2011).
27. R. A. Berner, *Science* **276**, 544-546 (1997).
28. M. Domeier, *Geoscience Frontiers* **9**, 789-862 (2018).
29. C. L. Colleps *et al.*, **19**, 257-271 (2018).
30. W. Cao, C.-T. A. Lee, J. S. Lackey, *Earth and Planetary Science Letters* **461**, 85-95 (2017).
31. J. Hartmann, N. Moosdorf, *Geochemistry, Geophysics, Geosystems* **13**, (2012).
32. K. J. Matthews *et al.*, *Global and Planetary Change* **146**, 226-250 (2016).
33. Y. Dilek, H. Furnes, *Geological Society of America Bulletin* **123**, 387-411 (2011).
34. Y. Dilek, H. Furnes, *Elements* **10**, 93-100 (2014).
35. C. R. van Staal *et al.*, **40**, 94-117 (2013).

36. F. A. Macdonald *et al.*, *American Journal of Science* **317**, 555-596 (2017).
37. M. Rioux *et al.*, *Earth and Planetary Science Letters* **451**, 185-195 (2016).
38. K. Burke, J. Dewey, W. Kidd, *Tectonophysics* **40**, 69-99 (1977).
39. H. Furnes, M. De Wit, Y. Dilek, *Geoscience Frontiers* **5**, 571-603 (2014).
40. A. C. Sengor, B. A. Natal'in, in *The Tectonic Evolution of Asia*, A. Yin, M. Harrison, Eds. (Cambridge University Press, Cambridge, 1996), pp. 486-640.
41. R. Hall, *Annual Review of Earth and Planetary Sciences* **45**, 331-358 (2017).
42. K. Wakita, *Journal of Asian Earth Sciences* **18**, 739-749 (2000).
43. C. Monnier *et al.*, *Geodinamica Acta* **12**, 43-55 (1999).
44. G. P. Yumul Jr, C. B. Dimalanta, E. J. Marquez, K. L. Queaño, *Journal of Asian Earth Sciences* **34**, 610-623 (2009).
45. J. Coggon, G. Nowell, D. Pearson, S. Parman, *Economic Geology* **106**, 93-117 (2011).
46. J. Encarnacion, E. Essene, S. Mukasa, C. Hall, *Journal of Petrology* **36**, 1481-1503 (1995).
47. D. Witts, R. Hall, G. Nichols, R. Morley, *Journal of Asian Earth Sciences* **56**, 77-104 (2012).
48. R. Hall, *Journal of Asian Earth Sciences* **20**, 353-431 (2002).
49. C. Parkinson, *Journal of Asian Earth Sciences* **16**, 13-28 (1998).
50. J. Hennig, R. Hall, M. A. Forster, B. P. Kohn, G. S. Lister, *Tectonophysics* **712**, 600-622 (2017).
51. S. C. Bergman, D. Q. Coffield, J. P. Talbot, R. A. Garrard, *Geological Society, London, Special Publications* **106**, 391-429 (1996).
52. A. Q. van Ufford, M. Cloos, *AAPG bulletin* **89**, 119-140 (2005).
53. S. L. Baldwin, P. G. Fitzgerald, L. E. Webb, *Annual Review of Earth and Planetary Sciences* **40**, 495-520 (2012).
54. W. B. Hamilton, *Tectonics of the Indonesian region*. (US Govt. Print. Off., 1979).
55. M. Cloos *et al.*, *Geological Society of America Special Papers* **400**, 1-51 (2005).
56. H. L. Davies, I. E. Smith, *Geological Society of America Bulletin* **82**, 3299-3312 (1971).
57. H. Davies, A. Jaques, *Geological Society, London, Special Publications* **13**, 341-349 (1984).
58. J. Ali, R. Hall, S. Baker, *Journal of Asian Earth Sciences* **19**, 535-546 (2001).
59. R. Hall, M. Audley-Charles, F. Banner, S. Hidayat, S. Tobing, *Journal of the Geological Society* **145**, 65-84 (1988).
60. P. Ballantyne, *Geological Society, London, Special Publications* **60**, 179-202 (1992).
61. C. Monnier *et al.*, *Mineralogy and Petrology* **65**, 1-28 (1999).
62. G. P. Yumul, *Island Arc* **16**, 306-317 (2007).
63. M. Pubellier *et al.*, *Journal of Southeast Asian Earth Sciences* **6**, 239-248 (1991).
64. G. P. Yumul Jr, C. B. Dimalanta, R. A. Tamayo Jr, D. V. Faustino-Eslava, *Journal of Asian Earth Sciences* **65**, 53-63 (2013).
65. R. Harris, *Gondwana Research* **10**, 207-231 (2006).
66. J. M. Pownall, M. A. Forster, R. Hall, I. M. Watkinson, *Gondwana Research* **44**, 35-53 (2017).
67. C. Monnier *et al.*, *Bulletin de la Société géologique de France* **174**, 529-543 (2003).
68. D. Cluzel, F. Jourdan, S. Meffre, P. Maurizot, S. J. T. Lesimple, *Tectonics* **31**, 1-18 (2012).
69. D. N. Reusch, *Geology* **39**, 807-810 (2011).

70. K. Nicholson, P. Black, C. J. T. Picard, **321**, 1-15 (2000).
71. S. A. Whattam, J. Malpas, I. E. Smith, J. R. J. E. Ali, P. S. Letters, **250**, 606-632 (2006).
72. K. Marsaglia *et al.*, **57**, 219-235 (2014).
73. W. Sivell, M. J. N. Z. J. o. G. McCulloch, Geophysics, **43**, 133-146 (2000).
74. D. Gray, D. J. T. Foster, **385**, 181-210 (2004).
75. A. Parsons *et al.*, *Geological Socety of America Bulletin* **131**, 274-298 (2018).
76. M. Colpron, J. L. Nelson, D. C. Murphy, *GSA Today* **17**, 1-7 (2007).
77. B. C. Burchfiel, D. S. Cowan, G. A. Davis, in *The Geology of North America*, B. C. Burchfield, P. W. Lipman, M. L. Zoback, Eds. (Geological Society of America, Boulder, 1992), vol. G-3, The Cordilleran Orogen: Conterminous U.S., chap. 8, pp. 407-479.
78. D. C. Murphy *et al.*, *Geological Association of Canada Special Paper* **45**, 75-105 (2006).
79. J. K. Snow, Y. Asmerom, D. R. Lux, *Geology* **19**, 629-632 (1991).
80. G. L. Farmer, D. J. J. J. o. G. R. S. E. DePaolo, **88**, 3379-3401 (1983).
81. J. W. Shervais, B. L. Murchey, D. L. Kimbrough, P. R. Renne, B. Hanan, *Geological Society of America Bulletin* **117**, 633-653 (2005).
82. J. Wakabayashi, *Tectonophysics* **568**, 230-247 (2012).
83. W. R. Dickinson, E. I. J. G. S. o. A. B. Rich, **83**, 3007-3024 (1972).
84. J. S. Pallister, J. R. Budahn, B. L. Murchey, *Journal of Geophysical Research: Solid Earth* **94**, 15901-15923 (1989).
85. R. Harris, *Geological Society, London, Special Publications* **60**, 301-325 (1992).
86. K. R. Wirth, J. M. Bird, *Geology* **20**, 75-78 (1992).
87. T. E. Moore, P. B. O'Sullivan, C. J. Potter, R. A. Donelick, *Geosphere* **11**, 93-122 (2015).
88. J. Lytwyn, J. Casey, S. Gilbert, T. Kusky, *Journal of Geophysical Research: Solid Earth* **102**, 10225-10243 (1997).
89. P. J. Haeussler, D. C. Bradley, R. E. Wells, M. L. Miller, *Geological Society of America Bulletin* **115**, 867-880 (2003).
90. Y. Isozaki, K. Aoki, T. Nakama, S. Yanai, *Gondwana Research* **18**, 82-105 (2010).
91. A. Ishiwatari, S. D. Sokolov, S. V. Vysotskiy, *Geological Society, London, Special Publications* **218**, 597-617 (2003).
92. N. V. Tsukanov, W. Kramer, S. G. Skolotnev, M. V. Luchitskaya, W. Seifert, *island Arc* **16**, 431-456 (2007).
93. J. Escuder-Viruete, A. Pérez-Estaun, M. Joubert, D. Weis, *Geologica Acta* **9**, (2011).
94. A. C. Kerr *et al.*, *Journal of Geophysical Research: Solid Earth* **107**, (2002).
95. A. C. Kerr, J. Tarney, *Geology* **33**, 269-272 (2005).
96. C. Lázaro *et al.*, *Journal of Metamorphic Geology* **27**, 19-40 (2009).
97. P. Mann, in *Sedimentary Basins of the World*. (Elsevier, 1999), vol. 4, pp. 3-31.
98. F. Sepúlveda, F. Hervé, M. Calderón, J. Lacassie, *Gondwana Research* **13**, 238-249 (2008).
99. M. Calderón *et al.*, in *Geodynamic Evolution of the Southernmost Andes*. (Springer, 2016), pp. 7-36.
100. G. M. Stampfli, G. Borel, *Earth and Planetary Science Letters* **196**, 17-33 (2002).
101. A. C. Şengör, J. Stock, *Geoscience Canada* **41**, 225-254 (2014).
102. H. S. Moghadam, R. J. Stern, *Journal of Asian Earth Sciences* **100**, 31-59 (2015).
103. R. Tirrul, I. Bell, R. Griffis, V. Camp, *Geological Society of America Bulletin* **94**, 134-150 (1983).

104. A. Michard, A. Chalouan, H. Feinberg, B. Goffé, R. Montigny, *Bulletin de la Société géologique de France* **173**, 3-15 (2002).
105. E. Bozkurt, J. A. Winchester, M. Satır, *Tectonophysics* **595**, 198-214 (2013).
106. A. I. Okay, O. Tüysüz, *Geological Society, London, Special Publications* **156**, 475-515 (1999).
107. A. M. Álvarez-Valero *et al.*, *Bulletin* **126**, 1614-1624 (2014).
108. M. Alavi, *Tectonophysics* **229**, 211-238 (1994).
109. W. Xiao, B. Windley, J. Hao, J. Li, *Journal of the Geological Society* **159**, 517-528 (2002).
110. M. Schwab *et al.*, *Tectonics* **23**, (2004).
111. E. Enkelmann *et al.*, *Tectonics* **26**, (2007).
112. T. N. Yang, Z. Q. Hou, Y. Wang, H. R. Zhang, Z. L. Wang, *Tectonics* **31**, (2012).
113. K.-J. Zhang, Y.-X. Zhang, X.-C. Tang, B. Xia, *Earth-Science Reviews* **114**, 236-249 (2012).
114. Q.-G. Zhai, B.-M. Jahn, R.-Y. Zhang, J. Wang, L. Su, *Journal of Asian Earth Sciences* **42**, 1356-1370 (2011).
115. R. A. Beck *et al.*, *Nature* **373**, 55 (1995).
116. P. Bouilhol, O. Jagoutz, J. M. Hanchar, F. O. Dudas, *Earth and Planetary Science Letters* **366**, 163-175 (2013).
117. R. Hébert *et al.*, *Gondwana Research* **22**, 377-397 (2012).
118. O. Jagoutz, L. Royden, A. F. Holt, T. W. Becker, *Nature Geoscience* **8**, 475 (2015).
119. I. Metcalfe, *Journal of Asian Earth Sciences* **66**, 1-33 (2013).
120. J.-W. Zi *et al.*, *Lithos* **144**, 145-160 (2012).
121. P. Jian *et al.*, *Lithos* **113**, 767-784 (2009).
122. B. C. Burchfiel, Z. Chen, *Tectonics of the Southeastern Tibetan Plateau and its Adjacent Foreland*. (Geological Society of America, 2012), vol. 210.
123. R. Pedersen, M. Searle, A. Carter, P. Bandopadhyay, *Journal of the Geological Society* **167**, 1105-1112 (2010).
124. R. Allen *et al.*, **436**, 223 (2008).
125. H. Zwart, *Medd. Dan. Geol. Foren* **17**, 504-516 (1967).
126. U. Kroner, R. Romer, *Gondwana Research* **24**, 298-329 (2013).
127. A. J. Hartley, J. Otava, *Journal of the Geological Society* **158**, 137-150 (2001).
128. R. Gayer, J. Jones, *Proceedings of the Ussher Society* **7**, 177-179 (1989).
129. A. Schäfer, *Geologische Rundschau* **78**, 499-524 (1989).
130. M. Narkiewicz, *Geological Quarterly* **51**, 231-256 (2010).
131. E. Garzanti, M. Gaetani, *Sedimentary Geology* **151**, 67-87 (2002).
132. H. S. Moghadam, R. J. Stern, *Journal of Asian Earth Sciences* **91**, 19-38 (2014).
133. C. R. van Staal, S. M. Barr, J. Percival, *Tectonic styles in Canada: the LITHOPROBE perspective. Edited by JA Percival, FA Cook, and RM Clowes. Geological Association of Canada, Special Paper* **49**, (2012).
134. C. A. Ver Straeten, *From Rodinia to Pangea: The Lithotectonic Record of the Appalachian Region. Geological Society of America Memoir* **206**, 251-282 (2010).
135. A. Piqué, J. W. Skehan, *Tectonics* **11**, 392-404 (1992).
136. R. D. Nance *et al.*, **17**, 194-222 (2010).
137. M. Villeneuve, *Journal of African Earth Sciences* **43**, 166-195 (2005).
138. A. Pique, A. Michard, *American Journal of science* **289**, 286-330 (1989).

139. R. D. Dallmeyer, J. E. Wright, D. T. Secor Jr., A. Snoke, **97**, 1329-1344 (1986).
140. J. D. Gleason, P. J. Patchett, W. R. Dickinson, J. Ruiz, **107**, 1192-1210 (1995).
141. K. C. Misra, F. B. Keller, *American Journal of Science* **278**, 389-418 (1978).
142. S. Hollis *et al.*, *Journal of the Geological Society* **170**, 861-876 (2013).
143. R. Pedersen, H. Furnes, *Journal of Geodynamics* **13**, 183-203 (1991).
144. D. G. Gee, H. Fossen, N. Henriksen, A. K. Higgins, *Episodes* **31**, 44-51 (2008).
145. W. C. McClelland, S. J. Malone, W. von Gosen, K. Piepjohn, A. Läufer, *Zeitschrift der deutschen Gesellschaft fuer Geowissenschaften* **163**, 251-259 (2012).
146. H. P. Trettin, in *Geology of the Innuitian Orogen and Arctic Platform of Canada and Greenland*, H. P. Trettin, Ed. (Geological Survey of Canada, 1991), vol. 3, pp. 241-259.
147. H. Trettin, R. Parrish, J. Roddick, *Geological Survey of Canada Paper 92-2*, 3-30 (1992).
148. T. Pharaoh, *Tectonophysics* **314**, 17-41 (1999).
149. B. F. Windley, D. Alexeiev, W. Xiao, A. Kroener, G. Badarch, *Journal of the Geological Society of London* **164**, 31-47 (2007).
150. W. Xiao *et al.*, *Annual Review of Earth and Planetary Sciences* **43**, 477-507 (2015).
151. U. Bold, J. L. Crowley, E. F. Smith, O. Sambuu, F. A. Macdonald, *Lithosphere* **8**, 729-750 (2016).
152. E. F. Smith, F. A. Macdonald, T. A. Petach, U. Bold, D. P. Schrag, *Geological Society of America Bulletin* **128**, 442-468 (2015).
153. N. Dobretsov, M. Buslov, *Russian Geology and Geophysics* **48**, 71-82 (2007).
154. T. Cherkasova, A. Chernishov, Y. Goltsova, T. Timkin, R. Abramova, in *IOP Conference Series: Earth and Environmental Science*. (IOP Publishing, 2015), vol. 27, pp. 012002.
155. I. K. Kozakov *et al.*, *Geotectonics* **46**, 16-36 (2012).
156. C. Buchan, D. Cunningham, B. Windley, D. Tomurhuu, *Journal of the Geological Society of London* **158**, 445-460 (2001).
157. R. Van der Voo, D. J. van Hinsbergen, M. Domeier, W. Spakman, T. H. Torsvik, *Geological Society of America Special Papers* **513**, 589-606 (2015).
158. T. Donskaya, D. Gladkochub, A. Mazukabzov, A. Ivanov, *Journal of Asian Earth Sciences* **62**, 79-97 (2013).
159. A. Kröner *et al.*, *American Journal of Science* **310**, 523-574 (2010).
160. H. Liu, I. D. Somerville, C. Lin, S. Zuo, *Geological Journal* **51**, 627-651 (2016).
161. J.-X. Zhang *et al.*, *Tectonophysics* **570**, 78-101 (2012).
162. S. Song, Y. Niu, L. Su, X. Xia, *Gondwana Research* **23**, 1378-1401 (2013).
163. B. R. Hacker, L. Ratschbacher, J. Liou, *Geological Society, London, Special Publications* **226**, 157-175 (2004).
164. D. Cluzel, *Journal of Southeast Asian Earth Sciences* **7**, 195-209 (1992).
165. A. Ishiwatari, T. Tsujimori, *Island Arc* **12**, 190-206 (2003).
166. B.-F. Han *et al.*, *Bulletin* **122**, 627-640 (2010).
167. B. Wang *et al.*, **497**, 85-104 (2011).
168. F. Choulet *et al.*, **312**, 1098-1145 (2012).
169. D. Alexeiev *et al.*, **42**, 805-820 (2011).
170. A. Kröner *et al.*, **21**, 901-927 (2012).
171. D. Alexeiev *et al.*, **39**, 261-291 (2016).
172. D. Brown *et al.*, *Earth-Science Reviews* **79**, 261-287 (2006).
173. L. Zonenshain *et al.*, *Tectonophysics* **109**, 95-135 (1984).
174. P. Spadea, M. D'Antonio, *Island Arc* **15**, 7-25 (2006).

175. J. Proust, B. Chuvashov, E. Vennin, T. Boisseau, *Journal of Sedimentary Research* **68**, (1998).
176. A. J. Newell, V. P. Tverdokhlebov, M. J. Benton, *Sedimentary Geology* **127**, 11-29 (1999).
177. P. A. Cawood, *Earth-Science Reviews* **69**, 249-279 (2005).
178. R. Glen, *Geological Society of London, Special Publication* **246**, 23 (2005).
179. C. V. Spaggiari, D. R. Gray, D. A. Foster, *Geological Society, London, Special Publications* **218**, 517-539 (2003).
180. G. Rosenbaum, *Episodes* **35**, 187-194 (2012).
181. V. A. Ramos, M. Escayola, D. I. Mutti, G. I. Vujovich, *Geological Society of America, Special Papers*, 331-350 (2000).
182. C. Casquet *et al.*, *Earth-Science Reviews*, (2017).
183. M. P. Escayola, M. M. Pimentel, R. Armstrong, *Geology* **35**, 495-498 (2007).
184. R. E. Ernst, N. Youbi, *Palaeogeography, Palaeoclimatology, Palaeoecology* **478**, 30-52 (2017).
185. K. P. Norton, P. Molnar, F. J. G. Schlunegger, **204**, 510-517 (2014).
186. Y. Goddéris *et al.*, **42**, 151-162 (2017).
187. L. Johansson, S. Zahirovic, R. D. Müller, *Geophysical Research Letters*, (2018).
188. G. J. P. T. Hadley, **39**, 58-62 (1735).
189. A. Donohoe, A. J. C. E. P. Voigt, Mechanisms, 115-137 (2017).
190. E. Kalnay *et al.*, *Bulletin of the American Meteorological Society* **77**, 437-472 (1996).
191. D. G. Van Der Meer *et al.*, *Proceedings of the National Academy of Sciences* **111**, 4380-4385 (2014).
192. I. P. Montanez, *Geochimica et Cosmochimica Acta* **101**, 57-75 (2013).
193. J. Higgins *et al.*, *Geochimica et Cosmochimica Acta* **220**, 512-534 (2018).
194. D. L. Royer, Y. Donnadieu, J. Park, J. Kowalczyk, Y. Goddéris, *American Journal of Science* **314**, 1259-1283 (2014).
195. T. J. Crowley, *Oxford Monographs on Geology and Geophysics* **39**, 3-20 (1998).
196. R. A. Berner, Z. Kothavala, *American Journal of Science* **301**, 182-204 (2001).
197. L. Frakes, J. Francis, *Nature* **333**, 547 (1988).
198. T. H. Torsvik, L. R. M. Cocks, *Gondwana Research* **24**, 999-1030 (2013).
199. M. R. Saltzman, S. A. Young, *Geology* **33**, 109-112 (2005).
200. M. Hambrey, *Palaeogeography, Palaeoclimatology, Palaeoecology* **51**, 273-289 (1985).
201. E. Díaz-Martínez, Y. Grahn, *Palaeogeography, Palaeoclimatology, Palaeoecology* **245**, 62-81 (2007).
202. P. Isaacson *et al.*, *Palaeogeography, Palaeoclimatology, Palaeoecology* **268**, 126-142 (2008).
203. P. Fuentes, J. Díaz-Alvarado, C. Fernández, M. Díaz-Azpiroz, N. Rodríguez, *Journal of South American Earth Sciences* **67**, 40-56 (2016).
204. D. K. Brezinski, C. B. Cecil, V. W. Skema, R. Stamm, *Palaeogeography, Palaeoclimatology, Palaeoecology* **268**, 143-151 (2008).
205. J. t. Veevers, C. M. Powell, *Geological Society of America Bulletin* **98**, 475-487 (1987).
206. I. P. Montañez, C. J. Poulsen, *Annual Review of Earth and Planetary Sciences* **41**, 629-656 (2013).
207. C. R. Fielding, T. D. Frank, J. L. Isbell, *Resolving the Late Paleozoic ice age in time and space*. (Geological Society of America, 2008), vol. 441.

208. L. Frakes, N. Alley, M. J. I. G. R. Deynoux, **37**, 567-583 (1995).
209. J. Zachos, M. Pagani, L. Sloan, E. Thomas, K. Billups, *Science* **292**, 686-693 (2001).
210. B. De Boer, R. Van de Wal, R. Bintanja, L. Lourens, E. Tuenter, *Annals of Glaciology* **51**, 23-33 (2010).
211. L. C. Ivany, S. Van Simaeys, E. W. Domack, S. D. Samson, *Geology* **34**, 377-380 (2006).
212. A. L. Troedson, J. B. Riding, *Journal of Sedimentary Research* **72**, 510-523 (2002).
213. R. Dingle, M. Lavelle, *Journal of the Geological Society* **155**, 433-437 (1998).
214. J. Ehlers, P. L. Gibbard, *Quaternary International* **164**, 6-20 (2007).
215. H. Von Storch, in *Analysis of Climate Variability*. (Springer, 1999), pp. 11-26.
216. V. Puchkov, R. E. Ernst, M. A. Hamilton, U. Söderlund, N. Sergeeva, *GFF* **138**, 6-16 (2016).
217. D. V. Kent, G. Muttoni, *Proceedings of the National Academy of Sciences* **105**, 16065-16070 (2008).
218. C.-T. A. Lee, J. S. Lackey, *Elements* **11**, 125-130 (2015).

Acknowledgements:

Author Contributions: FAM and NLS-H designed the study. FAM and OJ constructed the ophiolite database. NLS and YP conducted the paleogeographic analysis and associated calculations. LEL performed the statistical analysis. FAM, NLS, and OJ wrote the manuscript with input from YP and LEL. **Competing interests:** None declared. **Data and materials availability:** A summary of the suture database is available in Table S1 with the ice latitude compilation provided in Table S3. The full suture database as well as the code associated with paleogeographic and statistical analysis is available at: https://github.com/Swanson-Hysell-Group/Arc_Continent_Analysis

Supplementary Materials:

Materials and Methods

References 31-218

Figures S1-S9

Tables S1-S4

Movie S1

10.1126/science.aav5300

Supplementary Materials for

Arc-continent collisions in the tropics set Earth's climate state

Francis A. Macdonald, Nicholas Swanson-Hysell, Yuem Park, Lorraine Lisiecki, Oliver Jagoutz

Correspondence to: francism@ucsb.edu

This PDF file includes:

Other Supplementary Materials for this manuscript include the following:

Materials and Methods

Ophiolite-bearing sutures

Individual ophiolite-bearing sutures marking arc-continent collisions were traced from georeferenced geological maps and a global lithological map compilation (*31*) in QGIS. The sutures were each captured at a similar spatial resolution (i.e. node spacing) so the lengths could be readily comparable. These suture lines (Fig. S1) were assigned a magmatic age range, a metamorphic age range, an exhumation age range, and a plate ID corresponding to a tectonic unit on Earth (Table S1). The sutures within the resultant shapefile were reconstructed from 520 Ma to the present along with the tectonic units utilizing the paleogeographic model of Torsvik and Cocks (*23*) in the spin axis reference frame (anchor plate ID of 1). This paleogeographic model was updated to include a revision to Ordovician Laurentia (*21*) and the Paleozoic of Asia, including the addition of the Kazakh terranes following the model of Domeier (*28*). We also compared this model with the Mesozoic and Cenozoic model of Matthews (*32*), which gave similar results for suture length through time. Reconstructions and suture length calculations within latitude bands (Figs. 2 & S2) utilized the pyGPlates function library and custom Python scripts documented within a Jupyter notebook that reproduces the analysis and development of the associated visualizations. Suture lengths were sampled at 5 Myr timesteps.

Ophiolites are formed at ocean-continent transitions (OCT), mid-ocean ridges (MOR), ocean interplate plumes (OIP), and subduction zone (SZ) settings, which includes both nascent forearcs and backarcs, and the lower crust of volcanic arcs (*33, 34*). SZ ophiolites are the most common in the geological record due to their higher preservation potential—because they form on the upper plate of a subduction zone they are typically thrust onto continental crust during collision. Ophiolites unrelated to subduction have a lower preservation potential because they are commonly on the lower plate when they enter a subduction zone and are more likely to be subducted.

The time span between formation, collision, and exhumation can vary between suture zones and ophiolites formed in different settings. For example, OCT ophiolites form during rifting, which can initiate 100 Myrs or more before collision, such as the Birchy Complex in Newfoundland (*35*) which formed during the opening of the Iapetus Ocean at ca. 565 Ma and was not exhumed until the Taconic orogeny at ca. 465 Ma (*36*). On the other end, dates on magmatism and metamorphism of the SZ Semail ophiolites are indistinguishable (*37*) and predate exhumation by less than 20 Myrs. Thus, due to ongoing subduction, magmatism can predate and persist through metamorphism of the ophiolite, and metamorphism and collision can predate and overlap with ophiolite exhumation. Here we are primarily concerned with the timespan of ophiolite exhumation, which is best constrained by dates on ophiolitic detritus in syn-orogenic basins, although the quality of age constraints on these syn-orogenic deposits varies between different suture zones. Within the compilation, we report maximum and minimum age constraints on ophiolite magmatism, metamorphism, and exhumation (Table S1).

Former ocean basins and arc-continent collisions are typically marked by ophiolites along a suture zone. In a classic Wilson cycle, an ocean closes with an arc-continent collision followed by a continent-continent collision. This scenario gives the possibility of at least two discrete ophiolite-bearing sutures within a simple orogenic belt. However, sutures are often considerably more complicated than the idealized view as is the case in recent ophiolite-bearing sutures in Indonesia and the Alpine-Himalayan orogenic system. Moreover, many of the MOR and OIP ophiolites in the compilation were accreted along subduction zones, and could have been exhumed both during accretion and then again during terminal collision. Additionally, many sutures have been reactivated or are “cryptic”, lacking significant ophioilites, which have been

presumably removed by tectonics and erosion. Cognizant of these complications, we have attempted to outline sutures by tracing positions of ophiolites, or when absent, the position of blueschist metamorphism or the boundary between tectonic domains that were previously separated by an ocean.

We have restricted our compilation of ophiolite-bearing sutures to the Phanerozoic because prior to that time both the preservation of these belts and the paleogeographic models to determine latitude are of relatively poor quality. Indeed, even over the Phanerozoic there appears to be a preservational bias to the modern with more ophiolite-bearing sutures in the Cenozoic (30 sutures in 65 Myr = 0.46 sutures per Myr) than in the Mesozoic (32 sutures in 185 Myr = 0.17 sutures per Myr) and Paleozoic (44 sutures in 290 Myr = 0.15 sutures per Myr) (Fig. S1). This is likely due not only to more complete preservation, but also to the fact that Cenozoic belts are more commonly broken up into multiple shorter sutures. For example, twelve separate sutures are distinguished in Indonesia, but if this belt were poly-deformed and exhumed after a continent-continent collision, it is likely that only two distinct sutures would be identified. Consequently the difference in total and peak suture length in the Cenozoic is not as biased towards the modern as the number of sutures. For example, the modern peak in total suture length is only ~50% greater than the Paleozoic and Mesozoic peaks in total active suture length (Fig. 2). Additionally, more complex geometries are outlined along many Cenozoic ophiolite-bearing sutures, whereas older, poly-deformed sutures tend to be outlined by simple lines between preserved outcrops, which would tend to decrease total suture length in poly-deformed orogenic belts. The plate reconstructions also do not fully account for internal deformation, including oroclinal bending, which also affects the preserved suture lengths and geometries.

Below we describe the assumptions we have made in each orogenic belt. We acknowledge that our characterization of the magmatic, metamorphic, and exhumation history of these belts is simplified, but these simplifications are needed for brevity and analysis. We start with the most recent and best-constrained sutures marking ocean closure and arc-continent collision in Indonesia, the Pacific, and the Alpine-Himalayan belt. These sutures reveal the extent in space and time of ophiolite generation and preservation before modification by subsequent orogenesis.

We have identified 106 distinct Phanerozoic sutures which is greater than the 57 sutures that Burke et al. (*38*) identified through all of Earth History or the ~10 ophiolite-bearing orogenic belts defined by Furnes et al. (*39*). The difference is that we have attempted to distinguish the closure of individual basins through individual arc-continent collisions. Although we can do this with some success through the Cenozoic, as we get back into Mesozoic and Paleozoic orogenic belts, we are forced to group some of these composite suture zones into single belts. Although Sengor and Natal'in (*40*) identified 75 sutures in Asia, we have grouped many of their individual sutures into composite suture zones. We do not include ophiolites that are not associated with suture zones in our compilation, for example, Tihama Asir, Macquarie, Taitao, and Iceland (*39*), because these have not been exhumed in arc-continent collisions. The definitions of suture shapes and exhumation timing within our compilation can deviate from collisions of individual tectonic units within the Torsvik and Cocks (*23*) model, but typically are in agreement and can be reconstructed through their assignment to a given associated tectonic unit.

Indonesia (sutures 58-68, 108-112)

We use the Indonesian orogenic system to refer to Mesozoic sutures in Borneo and Java (*sutures 59,66*), Miocene to present sutures in New Guinea (*sutures 60,61*), Halmahera (*suture 64*), Obi (*suture 63*), Sulawesi (*suture 65*) and the Philippines (*sutures 67,68*), and the ongoing collision between the Banda arc and Australia (*sutures 58,62*). We also include Cenozoic sutures of the Western Pacific in New Caledonia and New Zealand (*sutures 108-112*) with the Indonesian orogenic system. We do not include the Wolya arc in Sumatra and the Andaman Islands (*suture 82*) or the Bentong-Raub suture in the Malay Peninsula (*suture 80*) with the Indonesian orogenic system because they are genetically related to the Alpine-Himalaya belt.

The Indonesian orogenic system began with Late Cretaceous collisions between the Luconia-Dangerous Grounds of Eurasia and continental blocks rifted from Australia (Banda, Inner Banda, and Argo), which form present-day Borneo and western Sulawesi (*41*). An ophiolite-bearing suture referred to as the Meratus belt (*sutures 59,66*) extends from Java (*42*) through eastern Borneo (*43*) to Palawan (*44*). Magmatic dates from the Meratus belt span 206-190 Ma (*45*), metamorphic dates have been reported between 145-34 Ma (*43, 46*), and exhumation occurred from the Early Miocene to present, driven in part by the collision between Palawan and the Philippines (*44, 47*).

After Late Cretaceous collision of the Banda blocks and Argo, subduction polarity reversed and a Cretaceous to Miocene SE-facing volcanic arc developed that was connected to the paleo-Sunda Arc (*48*). The ophiolites of Sulawesi (*suture 65*) were generated in this arc system (*25*) and the largest fragments of the East Sulawesi ophiolite were detached from their metamorphic sole in the late Oligocene (32-28 Ma; *49*) and thrust to the east above a west dipping slab (East Sulawesi block of Villeneuve et al., 2002). Uplift in Sulawesi and exhumation of these ophiolites accelerated in the Late Miocene (*50, 51*).

Further east, arc-continent collision began in New Guinea during the Late Oligocene to Early Miocene above a north-dipping slab (*52-54*). Two major ophiolite belts (*suture 60*)—the Irian-Marum ophiolite belts (including the April ultramafics), and the Papuan Ultramafic Belt (PUB)—are preserved along the Central and Peninsular Range. Exhumation of the Irian ophiolite began in the middle Miocene (16-14 Ma), and uplift in the Central Range accelerated from the Late Miocene to Pliocene (*55*). Although the PUB was generated and obducted earlier than the ophiolites in the Central Range (*56, 57*), it was also exhumed very rapidly over the past 10 Ma (*53*). In the paleogeographic models we assign these sutures to the colliding arc system and not Australia.

After arc-continent collision in New Guinea, a left-lateral strike-slip margin developed on the northern margin (*53*). Over the past 4 Myr, this change in plate motion extruded and exhumed the Cretaceous to Oligocene ophiolites of Obi (*suture 63*) (*58*), Halmahera (*suture 64*) (*59, 60*), and northern New Guinea (*suture 61*) (*61*).

The Philippine ophiolites have been grouped in four distinct belts (*62*). We combine belts 1 and 2 in an eastern suture zone (*suture 67*) and belts 3 and 4 in a western suture zone (*suture 68*). Belts 1 and 2 were juxtaposed in the eastern suture zone during left-lateral transpression, which resulted in Early Miocene uplift and deposition of coarse clastic sediments (*63*). The Palawan microcontinental block and Philippine mobile belt collided during late Early Miocene to early Middle Miocene resulting into the emplacement of the western ophiolites (*64*). The age of metamorphism is middle Miocene, and exhumation and sedimentation extended from the Late Miocene to the present (Yumul et al., 2009).

Backarc basins in the Banda Sea opened starting at ca. 15 Ma (*41*). The ongoing arc continent collision became emergent in Timor (*suture 58*) and Seram (*suture 62*) over the last 5

Myr (*65-67*). In the paleogeographic models we assign these sutures to the Banda arc system and not Australia.

In the Western Pacific, the Koh ophiolite of New Caledonia (*suture 108*) is composed of ophiolites with magmatic ages of ~220 Ma that were obducted near the Eocene-Oligocene boundary (*68, 69*). In New Zealand, the Tangihua ophiolite (*suture 109*) is likely an extension of the New Caledonia suture (*70*) and because the constraints are better in New Caledonia, we use the age constraints from there. The Tangihua ophiolite is spatially overprinted by a younger suture zone (*suture 112*) that exhumed the Northland ophiolite during the Early Miocene (*71, 72*). On the South Island of New Zealand, the Dun Mountain ophiolite (*sutures 110,111*) formed in the Permian, was exhumed in the Cretaceous (*73, 74*), and later dismembered by the Alpine fault.

Cordilleran-Pacific (sutures 13-27, 87-89)

The Cordilleran-Pacific orogenic system extends for more than 25,000 km along the Pacific Rim. We include Mesozoic-Cenozoic sutures of East Asia, the North American Cordillera, the Caribbean, and the Andes with the Cordilleran-Pacific system. In the North American Cordillera, suturing began in the Middle to Late Permian between the Dunite Peak intra-oceanic arc and the Yukon-Tanana terrane (*75*). After the ophiolite obduction, subduction polarity reversed and the remaining Slide Mountain (Canada) and Havallah (United States) oceans (*sutures 17-20*) were subducted under the Yukon-Tanana and Sonomia (*76, 77*) terranes forming the Late Permian Klondike arc (*75*), until they collided with the Laurentian margin in the Early to Middle Triassic. Exhumation of the Slide Mountain-Havallah ocean tract is marked by Permian to Triassic unconformities and deposition of the Simpson Lake Group (*78*). Following collision and subduction polarity reversal, the Cordilleran margin of North America became an active margin from the Middle Triassic onwards (*77, 79*). Thus, we use an exhumation age of 265-230 Ma for these composite sutures. For the segment in the United States, we define the suture using the Sr isotope 0.706 line (*80*). Our suture overlaps with the Roberts Mountain allochthon tectonic unit of Torsvik and Cocks (*23*), because this tectonic unit does not differentiate Sonomia. Along this active Cordilleran margin an additional pulse of ophiolites (Coast Range, Ingalls, Josephine, Smartville, *suture 15*) were generated from 172-160 Ma (*81*). These ophiolites formed in an accretionary setting and thus have been episodically tectonized since their formation. We use an exhumation age defining the main episode of ultramafic olistostrome and lithic fragment deposition in adjacent basins from ca. 100 Ma (*82*) until 80 Ma (*77, 83*), although locally exhumation continued afterwards.

Further north, closure of Anguyuchum Ocean (*suture 16*) led to the obduction of several large ophiolite tracts (*84-86*). Exhumation ages from ca. 146-90 Ma are provided by deposition of foreland deposits on the North Slope that contain ophiolitic detritus (*87*). We continue the Anguychum suture through to Chukotka, the South Anyui suture, and the Verkhoyansk (*sutures 75,87,88*) of Russia, but because constraints are lacking in these belts, we use the parameters from the closure of the Anguychum Ocean.

The Paleocene-Eocene collision of the Yakatak block caused the broad uplift of the Resurrection ophiolite (*88*) in SE Alaska (*suture 21*). Ophiolites in this belt formed and were metamorphosed from ca. 68-50 Ma and were uplifted and eroded from ca. 50-35 Ma (*89*).

In Japan and Korea, subduction and accretion has persisted for the last 500 Myr (*90*); however, the Paleozoic sutures (*sutures 56,57,99*) are an extension of the Qaidam-Qinlian-Dabie

belt (*suture 55*) and we include these with the Central Asian orogenic belt (CAOB). For the Cordilleran-Pacific belt, we include Kamchatka (*suture 25*), Koryak (*suture 26*), and NE Japan (*suture 27*), which were all were exhumed within the last 40 Myr (*90-92*).

Ophiolites in the Caribbean and northern Andes (*sutures 14,22-24,89*) are of the OIP type (*39*), and originated from a Cretaceous LIP that formed during three magmatic phases at ca. 124-112 Ma, 94-83 Ma, and 80-72 Ma (*93-95*). These were in part accreted during Cretaceous east-dipping subduction and then extruded during the Cenozoic development of the Lesser Antilles volcanic arc above a west-dipping slab (*96*). Exhumation of these ophiolites was diachronous from the Cretaceous to present (*97*). We have kept the northern Andean (*suture 14*) active from 60 Ma until present, because transpression and exhumation continued after the main phase of foreland deposition as part of active Andean uplift (*97*).

In the Andean belt south of the Northern Andes suture, we only include the Patagonian ophiolites (*suture 13*), which formed from ca. 270-140 Ma (*98*) and were uplifted and eroded in an arc-continent collision from ca. 100-70 Ma (*99*). Paleozoic sutures between exotic terranes in the central and southern Andes are included with the Gondwanides, described below.

Alpine-Himalayan (sutures 30-42, 78-84, 100, 104-106)

The Alpine-Himalayan orogenic system, extends from Morocco in the west, through the European Alps, the Anatolides, Zagros, Makran, the Himalayas, around the syntaxis through the Malay Peninsula and into Sumatra spanning a length of ~10,000 km. The formation of ophiolites and obduction along suture zones encompasses the opening and closure of the Paleo- and Neo-Tethys oceans, and accompanying marginal basins (*100*). We restrict sutures of the Alpine-Himalayan orogenic system to those formed in Mesozoic to present, and include Paleozoic sutures with the Hercynian-Variscan belt and the CAOB.

The western Tethys sutures are marked by the Mesozoic Pan-Arabian ophiolites (*sutures 30,31,83,104*), the Mesozoic to Cenozoic Alpine-Pontides (*sutures 32,78*), and the Cenozoic Zagros, Inner Tarus, and Maghebrides (*sutures 79,105,106*). The Mesozoic Pan-Arabian ophiolites formed in an SSZ setting (e.g. Troodos, Kizildag, Semail, Neyriz, Nehbandan, Muslim Bagh, and Waziristan; Furnes et al., 2014) from 125-90 Ma (*37*) and were obducted onto Africa and Arabia during the the mid-Turonian to latest Campanian (90-72 Ma) Ayyubid orogeny (*101-103*).

The Alpine-Pontide belt (*suture 32,78*) spatially overlaps and overprints the Hercynian belt (*5,28*). Ophiolite generation in the Alpine belt occurred predominantly from 170-140 Ma (e.g. Betic, Chenaillet, Zermatt-Saas, External and Internal Ligurides, Calabrian, Corsica, Mirdita, and Pindos), during opening of the Alpine-Tethys Ocean (*39*). Subduction related metamorphism began in the Alpine Tethys by the Valangian (140-133 Ma), and uplift and erosion of the ophiolites above the Iberian plate and Eurasia occurred primarily from 50-30 Ma (*104*). In Turkey, ophiolites in the northern Sakarya zone (*suture 32*) are predominantly part of a north-dipping Triassic subduction-accretion zone that formed on the northern margin of the Paleo-Tethys (*105*), which was uplifted from the Maastrichian through the Eocene (*106*).

Ophiolites associated with the Maghebrides of northern Africa (*suture 79*) formed during Oligocene to Miocene extension, and were metamorphosed throughout the Miocene (*107*). These ophiolites are attached to the Kabylies plate which has been exhumed from the Miocene to present (*104*). To the east, in the Zagros and Inner Taurus belts (*sutures 105,106*), Cretaceous ophiolites of the Sanandaj-Sirjan Zone and Semail ophiolite (*sutures 30,31*) that were originally

uplifted and partially eroded in the Late Cretaceous, were later re-exhumed from the Miocene to the present (*108*). We distinguish the Cretaceous and Miocene to present sutures to account for two distinct exhumation events, but acknowledge in older suture zones these would likely be lumped into one event.

Himalayan sutures include the Early Mesozoic Kunlun and Jinsha belts (*sutures 36,38,39,42*), the Cretaceous Bangong-Nuijang, Sistan, and Quetta belts (*sutures 35,37,84*), and the Cenozoic Indus-Tsangpo and Shyok belts (*sutures 33-34*). Foreland basin deposition in the Songpan-Garze basin suggests that exhumation occurred in the Kunlun belt from 250-210 Ma (*109, 110*) and in the Jinsha belt from 230-195 Ma (*111, 112*). Reconstructing the NW Kunlun suture to the Qadam-Qilian tectonic unit in the reconstruction of Torsvik and Cocks (*23*) results in signigicant overlap with the Kazakh terranes at 250 Ma, which might imply there should have been more longitudinal separation between these groups of blocks. In the northern Himalaya, the Bangong-Nuijang belt (*suture 37*) overprints the West Jinsha belt (*suture 36*) and marks the collision between the Qiangtang and Lhasa blocks (*110*). Exhumation is constrained by Late Cretaceous (90-74 Ma) molasse deposits on the Lhasa block (*113, 114*). Further west, the Sistan suture (*suture 84*) formed during Late Cretaceous amalgamation of the Luz and Afghan blocks (*103*). The Quetta suture formed during Late Cretaceous on the northwestern margin of India, and was overlapped by shallow-marine strata by 49 Ma (*115*). The Indus-Tsangpo and Shyok sutures (*sutures 33-34*) closed between 50-35 Ma, marking the final collision between India and Asia (*116-118*). As this is part of the active Himalaya, we continue exhumation of these sutures to the present.

Many of the Himalayan sutures continue eastward through SE Asia. The Ailaoshan, Chengning-Menglian, and Bentong-Raub belts (*sutures 40,41,80*) are continuations of sutures between Eurasia and Sibumasu, and demarcate the easternmost extent of Cimmerian ribbon continent (*119-121*). The Shan States (*suture 100*) is the suture between West Burma and Sibumasu, which was active from 155-120 Ma (*119*). The Tsangpo suture continues southeast to the Mt. Victoria-Kawlun belt (*suture 81*) (*122*), and similarly has been exhumed from 40 Ma to the present. We include ophiolites in the Katha-Gangaw range of Burma with the Victoria-Kawlun belt. Further south and west, the Wolya arc (*suture 82*) formed at 95 Ma and is overlain by Campanian 83.5-70.6 Ma radiolarian cherts (*123*), which were uplifted and eroded from 60-40 Ma (*124*).

Alleghenian-Hercynian-Variscan (sutures 5, 28, 85, 92-93, 107)

In Europe, the Rheic Ocean closed (*sutures 5,28*) with subduction under Laurussia and the collision of the Amorican Spur and Gondwana during the Devonian to Carboniferous Hercynian (or Variscan) orogeny (*125, 126*). Subduction-accretion processes and generation of SSZ ophiolites in the Rheic Ocean occurred from 410-330 Ma. Hercynian-Variscan ophiolites with magmatic ages older than this age range, such as the early Ordovican Internal Ossa-Morena Zone ophiolite sequences in SE Spain, and the late Silurian to Early Devonian Kaczawa Mountains and Sleza sequences in Poland, formed in OCT or MOR settings (*39*) and were later accreted to the Laurussia margin. In Europe, the arrival of Amorica (*5*) created foreland basins between 380-360 Ma. This collision was followed by the collision of Gondwana (*28*), which created Hercyian-Variscan foreland basins beginning at 340 Ma in the Czech Republic (*127*) that remained active into the Westphalian (304 Ma) in South Wales (*128*) through the Stephanian (299 Ma) in Germany (*129*) and from the Middle Variscan through the Sephanian (~335-300 Ma) in Poland

(*130*). Final collision and exhumation is marked by the emplacement of 330-300 Ma post-kinematic granites (*126*).

The Avalonia-Amorica suture in Europe (*suture 5*) can be broadly extended across Eastern Europe and the Black Sea to the Aghdarband-Krasnovodsk, Tuarkyr, Fore Range, and Sevan-Akera belts (*suture 107*)(*40*). We refer to this suture as the Tuarkyr (*107*) after the Carboniferous arc-continent collision in Turkmenistan (*131*). Based on the interpretation of (*131*), we have assigned an an exhumation age of 330-300 Ma. After collision at 300 Ma, subduction steped outboard to the Alborz belt. We also extended the Variscan belt south of the Black Sea to the South Slope flysch basin, and the Waser, Rasht, and Svanetia-Talysh belts (*40*), and the Alborz belt in Iran (*suture 85*)(*132*). These sutures are currently tied to Baltica as they are associated with peri-Baltican tectonic units that are not included in the model of Torsvik and Cocks (*23*) until 250 Ma.

The Avalonia-Amorica suture in Europe (*suture 5*) can be correlated with the 390-350 Ma Neo-Acadian suture in New England and Canada (*suture 92*) between Avalonia and Meguma, which extends from Nova Scotia in the subsurface to Cape Cod, Massachusetts (*133*). In the northern Appalachians, exhumation of the Neo-Acadian belt is represented by Early to Middle Devonian deposition of the Catskill Delta (*134*), and continued foreland deposition on the midcontinent through the Early Carboniferous (390-350 Ma).

Although the closure of the Rheic ocean occurred during the Devonian to Early Carboniferous in the northern Appalachians, it occurred at the end of the Carboniferous in the southern Appalachians and West Africa due to the Carboniferous counterclockwise rotation of Gondwana (*135, 136*). The final closure of the Rheic Ocean is marked by the 335-295 Ma Ouachita-Alleghenian-Mauritantide belt (*sutures 93,113,114*) (*137, 138*). In North Africa, exhumation of the Mauritantide belt is constrained by foreland deposition that continued through the Carboniferous to Early Permian (*135*). In the southern Appalachians, kyanite metamorphism records hornblende cooling ages of 320–295 Ma (*139*) that is coincident with granite magmatism (*136*). Although the Ouachita-Alleghenian-Mauritanide belt does not preserve an ophiolite because much of the suture is buried under the Atlantic, we include it in our compilation due to the vast sediment with volcanic debris that it shed across North America and North Africa as well as tuffs found in these basins (*135, 140*). We follow Nance et al. (*136*) in the placement of the Alleghenian suture in West Africa and North America. The suture likely extends into Mexico and is responsible for the low-grade and amagmatic Ouachita orogen (*136*). For ease in alignment with the tectonic blocks, we have placed the suture in Mexico along the Caltepec fault zone between the Acatlan and Oaxacan complexes. We acknowledge that the Rheic suture could be further north and buried by Cordilleran Neogene volcanic arc rocks, as depicted by Nance et al. (*136*), but movement of the suture slightly north does not significantly change the suture length in the tropics, particularly considering the uncertainty in the Paleozoic placement of these Mexican blocks in paleogeographic models.

Taconic-Caledonide (sutures 1-4, 6-8, 90-91, 94-96)

The Appalachian orogenic front extends from Alabama, USA to Newfoundland, Canada. Both Iapetan rift related OCT ophiolites (e.g. Rowe belt and Birchy complex) and SSZ related ophiolites (e.g., Anniopsquotch, Bay of Islands, Betts Cove, Lac Brompton, and Thetford Mines) mark the Ordovician suture between Laurentia and allochthonous arc terranes (from north to south, Dashwoods, Moretown, and the Piedmont Zone). In New England and Newfoundland

(*3,4*), these ophiolites were obducted and exhumed in the Taconic orogeny from approximately 465-440 Ma (*36, 133*). We extend these parameters for exhumation south to the southern Appalachian segment (*suture 2*) (*141*), and north to Ireland and Scotland (*suture 7*) (*142*).

Further north, the Appalachian belt is broadly equivalent to the Scandinavian Caledonides (*suture 6*), which were separated with the opening of the Atlantic Ocean. Ophiolite generation associated with the closure of the Iapetus Ocean occurred between ca. 500-470 Ma, and a second event occurred from 445-435 Ma that generated back-arc ophiolites (*143*). The older, eastern belt was exhumed primarily in the Middle to Late Ordovician as the continuation of the Taconic orogeny (*144*). The younger, eastern belt was exhumed in the Silurian with the final arrival of Baltica to the Laurentian margin (*144*). The Caledonides extend northward through East Greenland and Svalbard (*suture 95,96*) (*144*) where the belt was later modified by Late Paleozoic strike-slip motion (*145*) and displaced remnants of the Iapetan Ocean to the Pearya Terrane of northern Ellesmere Island (*suture 1*)(*146, 147*). Although the Greenland and Svalbard segments do not contain ophiolites, we include them in our compilation due to the continuity of ophiolite-bearing sutures in regions with more complete exposure to the north and south.

The arrival of Avalonia to the Appalachian margin created the 421-400 Ma Acadian orogeny in North America and Europe (*sutures 8,90,91,94*)(*133*). For the Avalonia margins in Europe (*suture 94*), we use the parameters for the Acadian orogeny in Canada (*133*), and we do not demarcate the Thor suture as it had a transcurrent boundary known as the Tornquist zone (*148*).

Central Asian Orogenic Belt (sutures 43-57, 97, 99, 103, 115-117)

The Central Asian orogenic belt (CAOB) is situated between the Siberia, North China, Tarim, and Baltica. Its development involved the collision and accretion of a series of island arcs, ophiolites and continental blocks to the bounding cratons throughout the Paleozoic (*40, 149, 150*). Mongolia forms the core of the CAOB and was the site of Ediacaran to Cambrian arc-continent collision (*suture 49*) between the Ediacaran Agardagh-Khantaishir arc and the Tuva-Mongolia Terrane (*151*). An Early Cambrian age of exhumation is provided by ophiolitic detritus in foreland basin deposits on the Zavkhan Terrane (*152*). To the North, Tuva-Mongolia was juxtaposed against Siberia in the Ordovician along the Derba-Olkhon and Kutushiba sutures (*sutures 51,52*) (*153, 154*).

The Bayankhongor ophiolite (*suture 50*) also formed during the Neoproterozoic and was accreted to the Baidrag block in the Ediacaran to Cambrian (*155*); however, as it was on the lower plate during accretion, it may not have been significantly exhumed until Cambrian to Ordovician deposition and metamorphism of the Dzag schist (*156*), or even until the Mesozoic with closure of the Mongol-Okhotsk ocean (*157*). Indeed, the extensive preservation of the Bayankhongor ophiolite suggests that it did not experience significant Paleozoic erosion, and we use the Jurassic to Cretaceous ages and closure of the Mongol-Okhotsk (*suture 54*) for ages of exhumation (*158*). Further south, an ophiolite-bearing magmatic belt of the Transaltai (*suture 48*) collided with the Mongolian terranes during the Late Paleozoic with a 360-300 Ma age provided by ophiolite- and volcanic-detritus in foreland basin deposits (*159*). The amalgamation of the Transaltai zone was followed by the arrival of Tarim and South China in the Permian to Triassic (*150*), forming the Central Asian and Slonoker sutures (*suture 47, 103*) which mark southern boundary of the CAOB.

Early Paleozoic collision of the Kunlun and Altyn blocks with Tarim closed a Cambro-Ordovician ocean basin (*109*) forming the Kudi-Altyn suture (*suture 97*). Following stable Cambro-Ordovician platform deposition, Middle to Late Ordovician tectonism and foreland deposition occurred across the Tarim block in response to arc-continent collision (*160*). Termination of collision is marked by the occurrence of post-collisional Late Ordovician granites and a major Silurian unconformity (*28, 160*). We follow Domeier (*28*) and continue the timing of arc-continent collision in the Kudi belt to the North Altyn belt. After collision, subduction stepped back to the south, and north dipping subduction and accretion along this amalgamated complex continued into the Permian, terminating with the arrival of the Songpan-Garze belt (*110*). Together, this suture along with the Jinsha suture (*sutures 36,39*), mark the Triassic closure of the Paleo-Tethys.

The Qinlian suture (*suture 115*) marks the closure of the Qilian Ocean and a back-arc basin between the Silian-Gaidam block and the Alashan block. Collision of the leading edge of the arc terrane may have begun as early as 475 Ma as marked by detrital zircon in the foreland (*161*), whereas closure of the back-arc and exhumation of the arc occurred from 446-420 Ma as revealed from ophiolitic detritus in Silurian to Devonian flysch and molasse deposits (*162*). Although the collision may have begun earlier, we use a 446 Ma age as onset as constrained by the youngest ages on arc related magmatism and blueschist metamorphism (*162*).
Further east, the Dabie-Sulu suture was exhumed in the late Triassic to Jurassic during the final collision between North China and South China (*163*), and extends east to Japan and Korea (*sutures 56,57,99*) (*90, 164, 165*).

Kazakhstan is composed of Proterozoic cratonic fragments embedded within early Paleozoic arcs (*150*). A major challenge of reconstructing the early Paleozoic arc-continent collisions in Kazakhstan is restoring the post Devonian oroclinal bending. The sutures of Kazakstan were recently reviewed by Dormeier (*28*), which include the Ordovician-Silurian suture between Baidaulet-Aqbastau and Bozchekul-Chingiz (*suture 46*), the Ordovician suture between Kyrgyz North Tianshan and Chu-Yili (*suture 117*), the Late Ordovician suture between Kyrgyz Middle Tianshan and Kyrgyz North Tianshan (*suture 116*), the Ordovician to Devonian suture between Chu-Yili and Aktau-Junggar (*suture 44*), and the Late Paleozoic Junggar-Balkhash (*suture 45*) (*166*) and Tianshan-Tarim sutures (*suture 43*) (*167*).

The Maikhan-Kyziltas belt (*suture 46*) marks the composite Late Ordovician suture between the the Baidaulet-Aqbastau and Chingiz arcs and the Late Silurian suture between the composite arc terrane and Proterozoic basement of the Laba terrane (*168*). Because collision and exhumation of these arcs may have diachronous we extend exhumation from Late Ordovician to Silurian. Collision of the Baidaulet-Aqbastau and Chingiz arcs occurred in the Late Ordovician, when conglomerate and olistostromes were deposited in the Maikan-Kyziltas belt, with possible correlatives in the Chagantaolegai and Hongguleleng serpentinite mélanges (*168*). Devonian collision between the composite arc terrane and the Laba terrane is marked by the olistostroms and ophiolitic remnants in the Silurian Mayila mélange (*168*).

The Ordovician suture between Kyrgyz North Tianshan (KNT) and Cambrian Chu-Yili (*suture 117*) is defined by ophiolitic rocks that are thrust to the southwest above KNT sometime during the Early Ordovician. A minimum age constraint on deformation and exhumation is provided by Middle Ordovician limestones that overlie the ophiolitic mélange (*169*) and ca. 470 Ma post-kinematic granites and Ar-Ar mica cooling ages on gneisses (*28, 170*).

The Late Ordovician suture between Kyrgyz Middle Tianshan and Kyrgyz North Tianshan (*suture 116*) is marked by Ordovician ophiolites along the northern slope of the Chatkal Range

(*171*). Arc magmatism was active from 467-445 Ma with high-grade metamorphism at ca. 450 Ma (*171*). A minimum age constraint on uplift and erosion is provided by unmetamorphosed Silurian strata, which unconformably overlie the ophiolite (*171*).

The Ordovician to Devonian suture between Chu-Yili and Aktau-Junggar (*suture 44*) is distinguished by Ordovician arc rocks on Aktau-Junggar that were metamorphosed during the Silurian to earliest Devonian (443–413 Ma) (*28*). This may be equivalent to the collision between the composite arc terrane and the Laba terrane on the other side of the orocline (*suture 46*). Ophiolites north of Aktau-Junggar are poorly constrained and may be associated with Late Paleozoic accretion or the northern limb of the orocline, and are thus not included in the sutures database.

The Tianshan-Tarim belt (*suture 43*) formed during the Carboniferous arrival of Tarim to the southern end of the Kazhakstan collage. These amalgamated terranes were subsequently oroclinally bent and collided to form the Junggar-Balkhash belt (*suture 45*), which was exhumed between 316-270 Ma (*166*).

The western boundary of the CAOB is marked by the Urals, which define a >4000 km arc-continent collision that extends from the Kara Sea to Kazakhstan (*172, 173*). The remnants of the Early Paleozoic subduction-accretion complexes occur in a belt (*suture 29,53*) between the East European and the West Siberian cratons (*174*). Magmatism and ophiolite generation in the Magnitogorsk arc and equivalents spans 488-392 Ma and was exhumed between 375-358 Ma during the early Uralian arc-continent collision with Baltica (*172*). Kazakhstan and Siberia collided with the eastern margin of the arc forming the Permo-Carboniferous Uralian suture (*173*). We constrain exhumation with deposition within the Uralian foreland basin from the Moscovian (*175*) to the Capitanian (*176*) (315-265 Ma).

Terra Australis and Gondwanides (sutures 9-12, 98)

The Terra Australis orogeny (*177*) refers to the ~18,000 km Paleozoic orogenic belt that developed on the margin of Gondwana, and is succeeded by the Late Paleozoic to Mesozoic Gondwanides. In eastern Australia, these orogenic events are lumped into the Tasmanides, and include a collage of orogenic belts that formed during a time span of ~300 Myrs (*178*). Although the active margin included South America, Australia, Antarctica, and South Africa, we do not include suture in Antarctica because of lack of information, and we do not include sutures for South Africa because there are no ophiolites or sutures preserved in the Cape Fold Belt. For our purposes, these omissions likely do not create a significant bias because the active margin of Gondwana was at high latitudes, outside of the tropical weathering belt, throughout the Paleozoic and Mesozoic.

In Australia, we demarcate two main ophiolite-bearing sutures, the early Paleozoic West Tasmanides (*suture 10*) and the late Paleozoic to Mesozoic East Tasmanides (*suture 9*). Magmatism associated with the ophiolites in the West Tasmanides is mostly Cambrian, and these belts were exhumed from the Ordovician to Silurian (*179*). The East Tasmanide ophiolites are predominantly accretionary and were exhumed during oroclinal buckling from 260-240 Ma (*180*).

The Pampean belt and the eastern ophiolite belt (*suture 12*)*(181)* originated from Africa in the Neoproterozoic and were transplanted during the Cambrian to the Rio de Plata craton and Amazonia (*182, 183*). Ophiolites in the Pie de Palo belt, or Chuscho (*suture 98*), formed during the Proterozoic and were obducted during the Middle to Late Ordovician during the collision

between Cuyunia and the Famatanian arc (*181*). The western ophiolite belt, or Sierra del Tigre (*suture 11*)(*181*), also formed between the Cambrian and Ordovician and was exhumed during the Devonian to Carboniferous during the collision of Cuyunia and Chilenia.

Large Igneous Provinces

Outlines of large igneous provinces (LIPs) through the Phanerozoic (Fig. S3) were taken from the compilation of Ernst and Youbi (*184*), and emplacement ages were modified from the literature (Table S2). The compilation of Ernst and Youbi (*184*) seeks to reconstruct the original areal extent of LIPs with the caveat that there can be significant uncertainty with doing so, particularly for older more deeply eroded LIPs. The paleogeographic positions of the LIPs were reconstructed using the same paleogeographic model used for the ophiolite-bearing sutures. Python functions from the pyGPlates library as well as custom functions were used for the analysis.

The post-emplacement weathering and erosional history of each LIP should be dependent on the tectonic and climatic setting that each LIP experiences during and after emplacement. For example, if a LIP is emplaced into an actively rifting basin and is quickly buried by sediments, its ability to consume CO_2 through silicate weathering could be significantly attenuated soon after burial. In a similar manner, without active uplift, soil shielding from regolith development on low-relief LIPs could significantly decrease the local weatherability of a LIP and mute its impact on global weatherability (*10*). Furthermore, the thickness of this regolith is dependent on the local climate (*185*). However, it is difficult to constrain when and how much each of these factors affect the post-emplacement weathering and erosional history of each LIP—in many cases the timing and extent of burial of LIPs emplaced into actively rifting basins is poorly constrained, and the timing, extent, and effect of regolith development on LIP weatherability is difficult to model. Ultimately, however, we expect all LIPs to effectively cease consuming appreciable atmospheric CO_2 at some point after emplacement, either through burial or consumption of the majority of weatherable material.

In order to account for these post-emplacement weathering and erosional histories, we imposed two post-emplacement scenarios on our calculated LIP areas (Fig. S4). In the "decay" scenario, the areas of all LIPs decay exponentially after emplacement. This approach follows that of Goddéris et al. (*186*) wherein the original and present-day area of five Phanerozoic LIPs were compared and exponential decay was assumed. In the analysis of Goddéris et al. (*186*) half-lives of the LIPs were observed to be between 90 to more than 400 Myr, with three of the five half-lives clustering at ~120 Myr. In our analysis, we take a half-life of 120 Myr as reasonable to first order, and use this value as the exponential decay half-life of the LIPs. In the "decay+burial" scenario, LIPs associated with successful rifting, associated thermal subsidence, and geological evidence for at least partial sedimentary cover soon after emplacement were instantly removed from the paleogeographic reconstruction, while all other LIPs were treated the same as in the "decay" scenario. In a successful rift, the timescale of burial of extrusive volcanics by sediments due to subsidence may vary from 0 to ~10 Myr depending on relative sea level, geometry of the rift and associated volcanics, and timing of emplacement relative to the rift-drift transition. Thus, we use instantaneous burial as an end-member estimate for burial after emplacement. The LIPs deemed to be associated with successful rifting and subsidence are: CAMP, NW Australia Margin, Parana-Etendeka, Seychelles, North Atlantic Igneous Province, and Afar (Table S2).

Our LIP reconstruction differs from that of Johansson et al. (*187*) in several respects. In contrast to the decay and decay+burial scenarios, Johansson et al. (*187*) uses a static extent for

each LIP throughout the reconstruction with some of the polygons corresponding to the present-day surface extent and some of the representing the original extent that includes currently buried portions of the LIP (e.g. the North American Midcontinent Rift). The LIP compilation we utilize seeks to outline the original extent of the LIPs through use of the area of associated dikes and sills. The LIP reconstruction used in this study includes pre-Phanerozoic LIPs. However, given the imposed exponential decay since emplacement, the inclusion of these LIPs do not significantly impact the calculated LIP areas, as can be seen by the small area of LIPs prior to ca. 380 Ma in Fig. S4.

In the "decay" scenario, we observe three primary peaks and one minor peak in calculated LIP area within the tropics (Fig. S4B). The first primary peak starting ca. 511 Ma is associated with the emplacement of the Kalkarindji, the second primary peak starting ca. 380 Ma is associated with the emplacement of the Kola-Dnieper, and the third primary peak starting ca. 201 Ma is associated with the emplacement of the Central Atlantic magmatic province (CAMP). A Cenozoic peak is associated with both the ca. 30 Ma emplacement of the Afro-Arabian (Afar) LIP as well as the effect of the earlier drift of the Deccan LIP into the tropics. In the "burial" scenario, the peak associated with the CAMP is absent, but the other peaks remain (Fig. S4).

Definition of the tropical rain belt

The meridional overturning circulation in the tropics known as the Hadley circulation (*188*) results in the tropics being a region of intense convective precipitation (Fig. S5). The location of the precipitation maximum within the tropics is referred to as the intertropical convergence zone (ITCZ) which is associated with the ascending branch of the Hadley circulation (*189*). As a result of the ITCZ, and its migration through the year, annual rainfall on Earth is greatest within ~15º of the equator resulting in the tropical rain belt (Fig. S5). Weathering rates within basaltic watersheds in the warm and wet tropics are approximately an order of magnitude higher than those in mid-latitudes (Dessert et al., 2003). The tropical rain belt contrasts with the arid subtropics where the same overturning circulation of the atmosphere results in dry descending air. Geologic and paleomagnetic data reveal a consistent latitudinal position of evaporite deposits in the subtropics (~20-30º) over the past 2 billion years (*14*) indicating that this descending circulation is a long-lived feature of Earth's climate. These data also indirectly constrain the ascending branch of the Hadley circulation to have been confined to the equatorial region throughout Earth history. Shifts in the position of the ITCZ are associated with asymmetries in the hemispheric energy budget of the atmosphere both during the seasonal cycle and on longer timescales (*189*). Given that hemispherically asymmetric forcings are relatively small, the position of the ITCZ is interpreted to be stable even with large changes in forcing resulting from changing CO_2 levels (*189*). As a result of these dynamics and the geologic record, intense precipitation within the tropical rain belt is best interpreted as a persistent long-term component of Earth's climate. Figure S5 plots global precipitation and temperature zonal mean values taken from the NCEP/NCAR reanalysis 1 project (*190*). In modern climate data, the region within 10º of either side of the equator corresponds with precipitation greater than 1.5 m/yr and the region within 15º corresponds with precipitation greater than 1.0 m/yr. In our analysis of the suture length in the tropical rain belt, we consider suture length within 10º, 15º and 20º of the equator. While tropical precipitation is most intense within 5º of the equator, the rates exceed anywhere else on earth within 15º and wider definitions of the belt of 15º and 20º are likely more appropriate than narrower ones given uncertainty associated with assigned suture ages and paleogeography.

Phanerozoic ice extent

Previous attempts to compare changes in CO_2 sources or sinks to climate change through the Phanerozoic have relied on pCO_2 or temperature estimates from proxy data (*19, 21, 187*) or geochemical box models (*18, 191*). Although organic proxies coupled with oxygen and boron isotopes of benthic foraminifera provide consistent and relatively robust records of climate over the Cenozoic (*24, 26*), prior to that, direct estimates of pCO_2 rely on paleosols and leaf stomata with variable data density that is particularly lacking in the Paleozoic (*24, 192*). pCO_2 estimates from box models are based primarily on records from shallow water or terrestrial carbonates that are compromised by local processes and alteration (*193*) and are sensitive to assumptions regarding biogeochemical cycling in deep time (*194*). Although the shape of the pCO_2 curve from 400 Ma to present (*24*) is broadly consistent with the geological record of latitudinal extent of continental ice (*195*), both the models based on terrestrial proxy data (*24*) and geochemical box models (*196*) fail to predict the end-Ordovician glaciation. Consequently, we use the latitudinal extent of ice as the most robust measure of the long-term climate state to compare to our records of sutures in the tropics.

Since the compilation of Crowley (*195*), there have been significant revisions to the geological timescale and paleogeographic constraints on climatic indicators. Consequently, we have updated a database on the latitudinal extent of continental ice sheets, excluding Alpine glaciers and ice rafted debris, as described below. We report ice extent as maximum extent of latitude from either pole (Table S3) and translate that into a latitude of ice in Figure 2C. For every million-year age pick, we have attempted to determine the maximum extent of ice from the literature. If the million-year pick was at or near a transitional interval between two periods of different ice extent, we used a midpoint between the two ice extents to the nearest 5º from the poles. Other than these midpoint picks through transitions, our latitudinal resolution is at the nearest 10º. For comparison to our tectonic proxy records, we then subsampled the record of ice extent at a 5 Myr resolution. We chose this resolution not only because it matches the resolution of our tectonic records, but also because it avoids much of the uncertainty about ice-extent on the ~1 Myr timescales.

Over the Phanerozoic there have been three major glaciations, in the Late Ordovician, Permo-Carboniferous, and the Cenozoic, with a smaller glacial advance in the Late Devonian. Frakes et al. (*197*) suggested that the Ordovician ice-sheets extended from the pole to beyond 60ºS from 458-428 Ma. Chatfieldian (starting at ~454 Ma) glacial deposits have been identified in Morocco, which was at ~70ºS during the Late Ordovician (*198*), and corresponds to the beginning of significant eustatic change (*199*). Katian (~453-445 Ma) glacial deposits have also been described in Peri-Gondwanan terranes in Europe and the Canadian Maritimes (*200*), which were above 60ºS in the Late Ordovician (*198*). We follow (*199*) and define the initiation of glaciation to 80ºS at the Middle-Late Ordovician boundary (458 Ma) with an expansion to ~70ºS by 454 Ma and to 60 ºS by 452 Ma. During the Hirnantian glacial maximum from 445.2 to 443.8 Ma, ice extended to ~40ºS in Arabia (*198, 200*). Silurian glacial deposits are described as Rhuddanian (ending by ~439 Ma) in South America, which was also at ~60ºS (*200, 201*). Thus, we use a glacial extent of 30º from the pole from 452-447 Ma with a Hirnantian glacial maximum to 50º from the pole from 445-444 Ma, which we ramp up and down in 10º per million year increments (Table S3).

Late Devonian glacial deposits have been identified in Peru, Bolivia, Brazil, and central Africa (*202*). Reconstructions of Gondwana place Peru and Bolivia at or below 60ºS during the

Latest Devonian to early Carboniferous (*23*) whereas glacial deposits in Brazil and central Africa only extended to ~70ºS. Late Devonian glacial deposits are limited to the second half of the Fammenian (*202*), which spans ~365-359 Ma. A glacial origin for the deposits in Peru and Bolivia is demonstrated by abundant dropstones and striated clasts; however, grounded ice has not been identified at these sites. Instead, these glaciomarine deposits are sourced from highlands in Chile and Bolivia (*23*) associated with Devonian-Carboniferous accretionary events on the active Gondwanan margin (*203*). Devonian-Carboniferous glacial deposits from alpine glaciers have also identified in the Appalachians (*204*). Thus, although there was cooling during the Latest Devonian to early Carboniferous, it is not clear that a continuous ice sheet extended from the South Pole to above 60ºS, and instead the polar ice cap may have been limited to high-latitude sites with grounded ice in Brazil and Africa, which smaller Alpine ice sheets present in the Precordillera and Appalachian. Consequently, we limit the ice extent to for the Late Devonian glaciation to 80ºS from 365-361 Ma, with an ice advance to 70ºS from 360-359 Ma, a retreat to 80ºS at 358 Ma reflecting early Tournaisian glacial deposits in Brazil (Table S3), and ice free after 358 Ma.

Ice was present in eastern Australia by 331 Ma (*195, 205-207*), which was >40º from the southern pole (*198*). Although there may have been some ice earlier in South Africa and western South America, the former is uncertain and the later may have been from Alpine glaciers. Earlier reconstructions have suggested the presence of Visean (345-331 Ma) ice sheets (*195, 205-207*) and consequently we ramp ice extent by 5º every million years between 338 Ma and the 40º ice-extent of 331 Ma, and use ice-free conditions from 357-338 Ma. The Gondwanan ice sheets expanded during the Middle Pennsylvanian, reaching a glacial maximum at ~50º from the southern pole by 309 Ma (*198*) when ice extended to Brazil, the Arabian Peninsula, and Central Africa (*206*). The glacial maximum persisted through the Permo-Carboniferous boundary (ca. 299 Ma), but ice volume decreased after 299 Ma, and ice was restricted to Australia after 293 Ma (*206, 207*). By the Early Permian, Australia had drifted to higher latitudes and was largely above 60ºS (*198*). Glaciation persisted in Western Australia until ~277 Ma and in Southeastern Australia until ~260 Ma (*206, 207*). We use a >20º latitude for ice extent in Western Australia in the Permian, and >10º latitude for ice extent in Southeastern Australia in the Permian. To describe this retreat in ice extent between 50º and 20º, we decreased the ice extent by 5º every million years between 299 and 293 Ma. We used a 20º ice-extent between 293 and 278 Ma, a 15º ice-extent at 277 Ma, and a 10º ice-extent between 276 and 260 Ma (Table S3).

Frakes et al. (*208*) reported evidence of Lower Cretaceous glaciation in Australia, but no grounded ice has been identified, so we do not include Cretaceous glaciation in our compilation.

Cenozoic glaciation is classically defined by the initiation of Antarctic ice at 34 Ma to present, although eustatic fluctuations suggest that there may have been ephemeral ice by 35 Ma (*209*). Oxygen isotope records coupled with ice sheet models suggest that the volume of ice in Antarctica was near that of today during the Early Oligocene but decreased by at least 50% from the Late Oligocene to Middle Miocene (~25-14 Ma) (*209, 210*). The modern extent of grounded ice ~30º from the poles is anchored by the glaciation of Greenland and the Antarctic Peninsula. Greenland was not glaciated until the Pliocene, and although there was grounded ice on the Antarctic Peninsula during the Early Oligocene (*211*), the Antarctic Peninsula remained ice free from the Late Oligocene through the Middle Miocene (*212, 213*), but received ice rafted debris, suggesting much of Antarctica was still glaciated. Thus, we use an ice extent of 10º from 37-35 Ma and 30º from 33-27 Ma, 20º from 25-15 Ma, and then increasing to 30º by 13 Ma, with transitions at 20º at 34 Ma and 25º at 26 Ma (Table S3).

Ice appeared in Greenland, British Columbia, and Chile by the Miocene-Pliocene boundary (*214*), and to the American Midwest during the Last Glacial Maximum, but the Cordilleran ice-sheets of British Columbia and Chile were largely Alpine, so are not appropriate for our compilation. It was not until ~2.58 Ma that ice extended to the mid-continent as a low-relief ice sheet, with additional growth near the end of the Matuyama magnetic polarity chron at ca. 1 Ma (*214*). Thus, we keep ice-extent at 30º to 3 Ma, extend to 40º at 2 Ma, and to 50º at 1 Ma to present. Despite the fact that ice is currently at 30º from the pole, we keep it at 50º at 0 Ma to reflect the maximum ice-extent at the last glacial maximum.

Correlation between suture length and glaciation

Previous attempts to correlate changes in tectonic forcings with Phanerozoic climate change either did not employ statistics (*18, 30, 191*) or used a wavelet cross-correlation (*187*) with pCO_2 estimates or models. Along with issues relating to the fidelity of the pCO_2 estimates described above, because these datasets are strongly auto-correlated, direct cross-correlation techniques are not appropriate (*215*). That is, these treatments lack a null-hypothesis of a random or spurious correlation to compare with the proposed correlations between tectonic forcings and climate change.

To generate a robust null-hypothesis and test the statistical strength of the correlation between arc-continent collisions in the tropics and glaciation, four glacial intervals (representing the end-Ordovician, end Devonian, Permo-Carboniferous, and Cenozoic) were simulated to occur at random times throughout the past 520 Myr. These simulated records and the real record of glaciation were then compared to the suture length time series. This analysis accounts for the auto-correlation that exists in both datasets wherein values are related to the values preceding them. 10,000 synthetic records of the four glacial episodes were generated with the timing of where they occur within the 520 Myr time window re-arranged such that each of the four events occurs exactly once in each scenario (Fig. S6). A log-normal distribution was used to simulate different wait times between glacial events. An algorithm was generated for which there would be an equal chance of glaciation at any point over that time span. Because there are only four different glacial events, there are limited scenarios for glacial events at the start or end of the time window. To mitigate these edge effects, scenarios were permitted where the simulation starts or ends midway through one of the glacial events.

To minimize artifacts from uncertainties in the age models, the records of ice extent and tropical sutures were subsampled at a 5 Myr resolution. Each pick for ice extent represents the maximum extent ±2.5 Myr from the given age. For the ice record, there was little difference in the correlation statistics when we subsampled the record at 5-Myr time samples or used the average ice extent over a 5-Myr window.

Suture length in the tropics (<10º, <15º, and <20º latitude), total sutures, and suture length at high latitude (>40º latitude) were compared to both the synthetic records and the geological record of ice extent. The histogram plots (Fig. S7, right column) correlation coefficients (r) obtained when comparing suture length to the simulated ice extent records, and the colored dots show r when suture length is compared to the observed ice extent data. This analysis reveals a strong correlation between tropical and total suture length with ice extent, and a significantly weaker correlation between high-latitude sutures and ice extent (Fig. S7, right column). Suture length within 15º and 20º of the equator have more significant correlation metrics than total suture length or 10º from the equator, with the strongest correlation between sutures <20º latitude and ice extent ($p=0.0002$). The p-value of 0.0002 means that under the null hypothesis, only

0.002% of the random simulations of ice extent correlate with the <20º suture record as well as the observed data. In contrast, 55% of the random simulations correlate as well as the real data with the >40º suture record, which suggests effectively no relationship between high-latitude sutures and ice extent.

The amount of overlap in the suture database with glaciation was analyzed to determine if there were times with significant active sutures in the tropics when there was not glaciation. Glaciation was defined by continental ice extending beyond 10º from the poles. A significant length of active sutures was defined as 20% of the modern suture length for each scenario, which is ~20% of the maximum suture length at any time in the record. Throughout the record, a fixed threshold was used because the maximum/modern tropical and total suture length is comparable to that during peaks in the Permo-Carboniferous and Ordovician (Fig. 2).

The percent of time ice extended beyond 10º overlaps strongly with both suture length in the tropics and total suture length (Fig. S7, left column), with the strongest overlap at <10º ($p = 0.0031$), whereas suture length at high-latitude does not overlap strongly with the presence of ice ($p = 0.4305$). In the left column of Figure S7, the histogram bars are for the random simulations, that is, the null hypothesis that the presence of significant sutures and ice are unrelated, and the colored dots show the actual observation. For example, in the real data, ice sheets are present for 55% of the time that extensive sutures were present within 10º of the equator. The p-value of 0.0031 means that under the null hypothesis only 0.31% of the random samples have a 55% overlap with the 10º suture record. The <10º, <15º, and <20º latitude and total sutures all have significant overlap with the presence of ice with p-values <0.014, whereas the >40º latitude record gives a p-value of 0.43, which is not significantly different from the randomly generated datasets (Fig. S7; Table S4). In comparison, ice sheets are present only 40% of the time that the length of total sutures is >20% of the maximum. This is consistent with episodes of suturing outside of the tropics that create peaks in total sutures without causing significant climate change, such as the Mesozoic peak in total sutures (Fig. 2).

Although different scenarios for ice extent yield differences in the probability of correlation, the advantage of correlating extent as opposed to overlap is that the most extreme ice events have the most influence on the results. The disadvantage is that it relies more heavily on the accuracy of the age model.

To test the effect of age uncertainty in the suture database and paleogeographic models, age model uncertainty was simulated assuming a maximum aggregate uncertainty of 5 and 10 Myr in a random walk from the observed value for 1000 simulations (Fig. S8, Table S4). Because individual sutures and terrane reconstructions carry the age uncertainty, a more robust way to characterize the age uncertainty would be to vary individual suture ages; however, this method would be computationally challenging and spot checks of data from individual sutures suggest that individual uncertainties can manifest in changes in the aggregate peak at multi-million year time-scales. Thus, although this approach is simplified, it does provide a metric of how sensitive the analysis is to the aggregate age model. For both the 5 and 10 Myr uncertainty scenarios, the correlation coefficients between ice extent and suture length do not change substantially by adding age uncertainty (Fig. S8, Table S4) suggesting that the correlation statistics are not particularly sensitive to the exact age of the peaks in suture length.

Given the strong correlation between tropical sutures and ice extent, the correlation between total sutures and ice extent is expected because the peaks in total sutures largely match those of tropical sutures with the exception of the Mesozoic peak in total sutures (Fig. 2). Nonetheless, the stronger correlation of tropical sutures than total sutures with both overlap and ice extent,

coupled with the very weak to negative correlation between high-latitude sutures and glaciation, is consistent with the hypothesis that the latitude of arc-continent collisions is significant for setting global climate state.

Correlation between large igneous provinces and glaciation

Unlike the one-to-one correspondence between the extent of ophiolite-bearing sutures in the tropics and ice extent, the peaks in tropical LIP area do not clearly correlate with glacial intervals (Fig. S4). Particularly, this analysis does not result in a significant areal extent of LIPs in the tropics during or immediate before both the Late Ordovician and the Permo-Carboniferous glaciations. Additionally, there is no known glaciation associated with the CAMP. The 380 Ma Kola-Dnieper LIP (*216*) proceeds the ~365-359 Ma Late Devonian glacial advance, but is also closely associated with the Uralian orogeny. The drift of the Deccan traps into the tropics has been previously argued to be associated with a cooling climate and the initiation of Cenozoic glaciation (*15, 217*), and our results are consistent with this interpretation, although the Himalayan orogeny was also ongoing at that time.

To quantify the strength of the correlation, Phanerozoic ice extent was compared to the area of LIPs for the decay scenario and decay+burial scenario. For overlap, 20% of the maximum area of LIPs was defined as significant. In both scenarios, total LIPs at all latitudes and LIPs above and below 15º have a negative to zero correlation with ice extent, with the exception of the decay+burial at <15º, which has a slightly positive correlation coefficient of r=0.10 (Fig. S9, Table S4). Note that this correlation is much weaker than the correlations between ice extent and both total suture length and suture length in the tropics. These results do not appear sensitive to age uncertainty (Table S4). Similarly, relative to the null-hypothesis, the decay+burial at <15º has the smallest p-value, but it is several orders of magnitude larger than the p-values associated with suture length and only significant at the 15% confidence level (Table S4).

Correlation between continental arc magmatism and glaciation

As an alternative to the hypothesis that global weatherability controls the Earth's climate state, it has been proposed that the extent of continental arc-volcanism is the primary driver of long-term climate change (*18, 218*). This has been quantified with the abundance of preserved young detrital zircon in sediments relative to depositional age (*18*) and the length of continental arcs through time (*30*). As the former is binned in geological periods of variable durations averaging ~50 Myrs, it is not readily comparable to time-series records that are at an order of magnitude higher-resolution. Even a comparison of overlap between glaciation and a threshold of high cumulative young zircon frequency is problematic because the data steps are at boundaries between geological periods that are commonly defined by environmental and biological turnover. However, the compilation of Cao et al. (*30*) provided arc length through time that can be subsampled at a 5 Myr resolution, which is readily comparable to our records of suture length.

To quantify the strength of the correlation, Phanerozoic ice extent was compared to the average length of continental arcs of Cao et al. (*30*). Similar to the LIP decay+burial at <15º, the continental arc length record correlates with the record of ice extent (r=0.38), but again with a much weaker correlation coefficient than the suture records (Fig. S9; Table S4). For overlap between glaciation and arc length, <20, 30, 40, and 50% of the maximum relative to the minimum of arc length were used as threshold values (Table S4). Only the <40% threshold is

significant at the 95% confidence level ($p<0.05$), the <30 and 50% thresholds are significant at the 90% confidence level (i.e., $p<0.1$), and the <20% threshold is not at all significant ($p=0.28$).

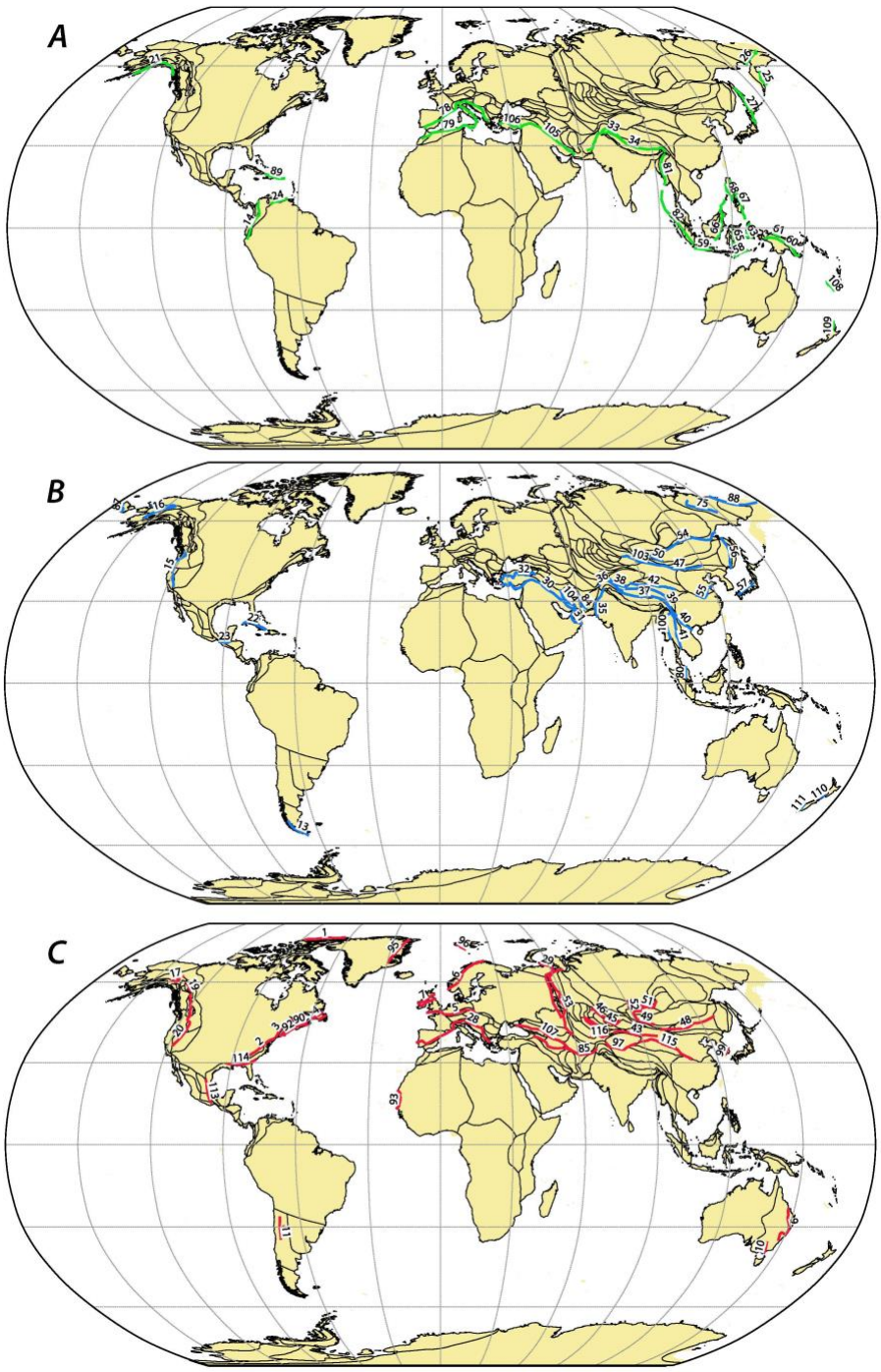

Fig. S1.

Numbered ophiolite-bearing sutures included in database for A) Cenozoic sutures in green, B) Mesozoic sutures in blue, and C) Paleozoic sutures in red. All sutures within the compilation are shown in present-day coordinates. Continental outlines shown are the tectonic units of Torsvik and Cocks (*23*) with modern coastlines for reference. Ages of the sutures are defined by the start date of exhumation.

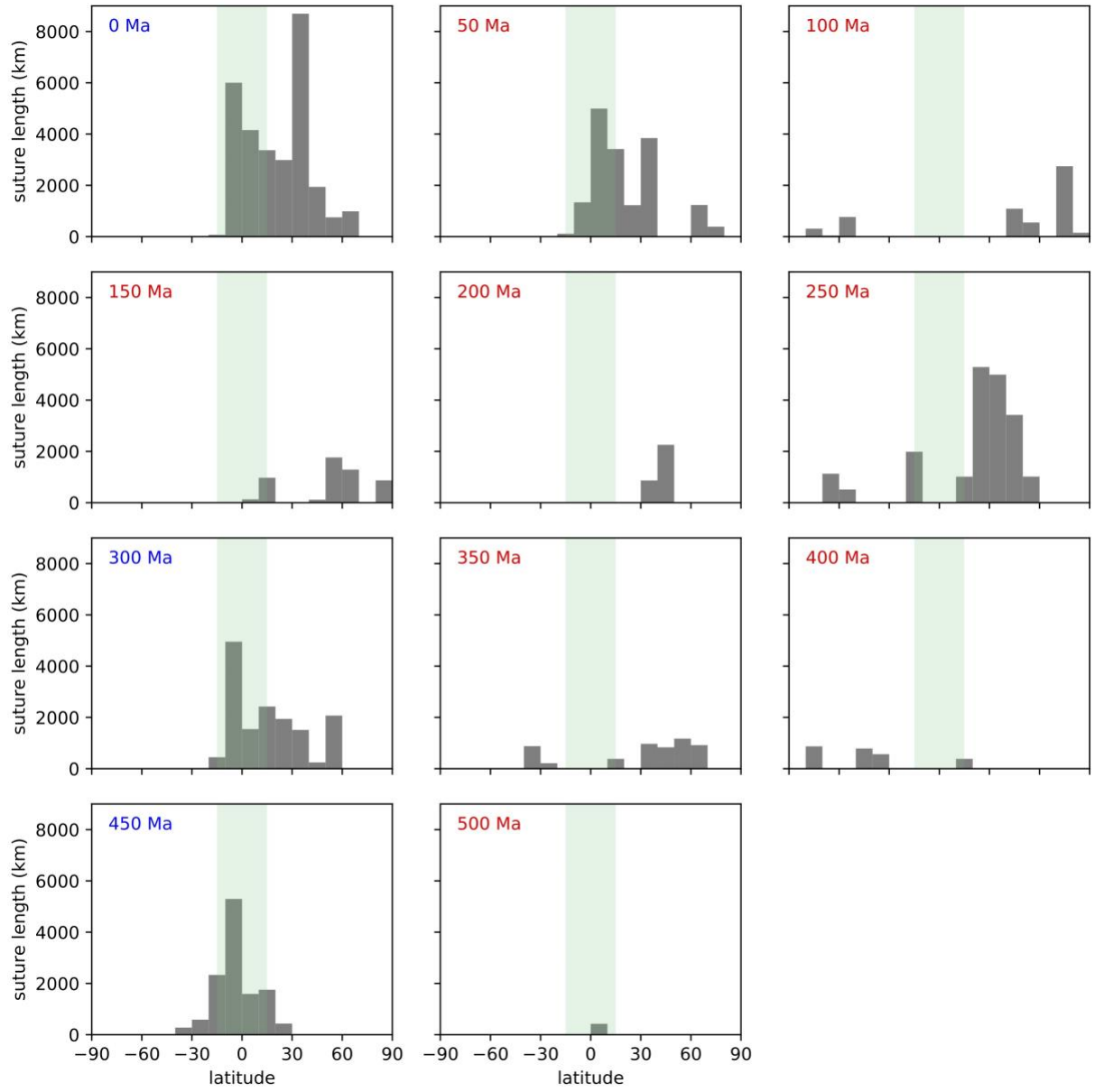

Fig. S2.

Bar plots of the latitudinal distribution of suture length in 50 Myr snapshots. Blue age labels are glacial intervals and red age labels are non-glacial intervals.

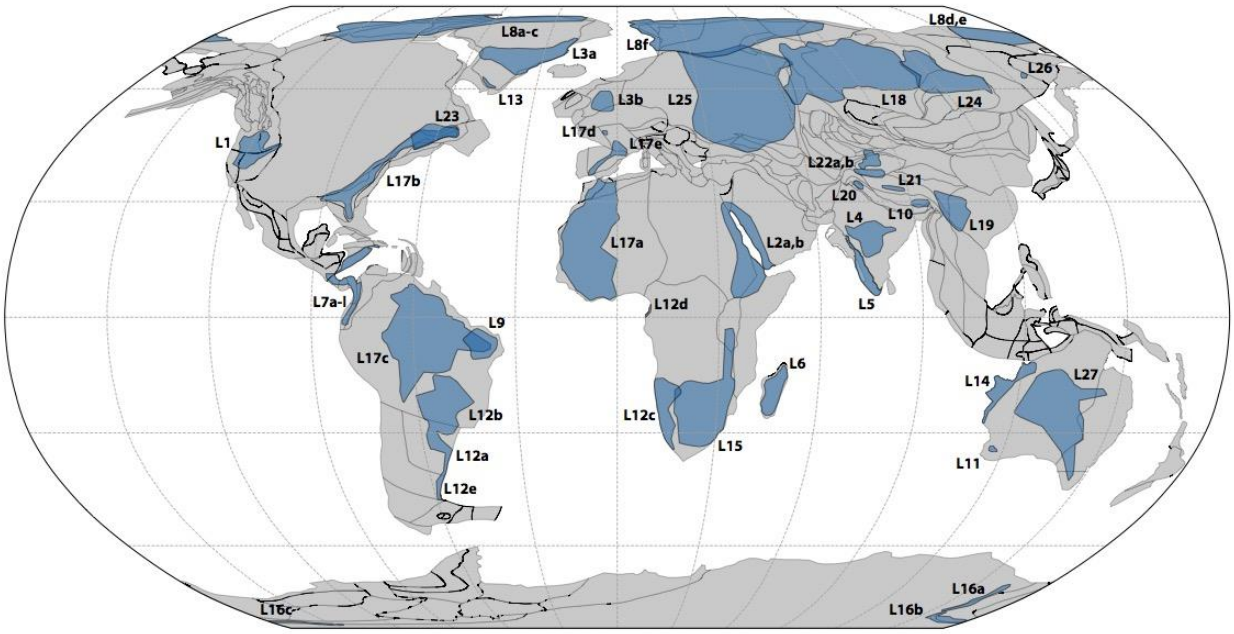

Fig. S3.

Numbered large igneous provinces included in database. Outlines of large igneous provinces through the Phanerozoic were taken from the compilation of Ernst and Youbi (*184*) and emplacement ages were modified from the literature. All large igneous provinces within the compilation are shown in present-day coordinates. Continental outlines shown are the tectonic units of Torsvik and Cocks (*23*).

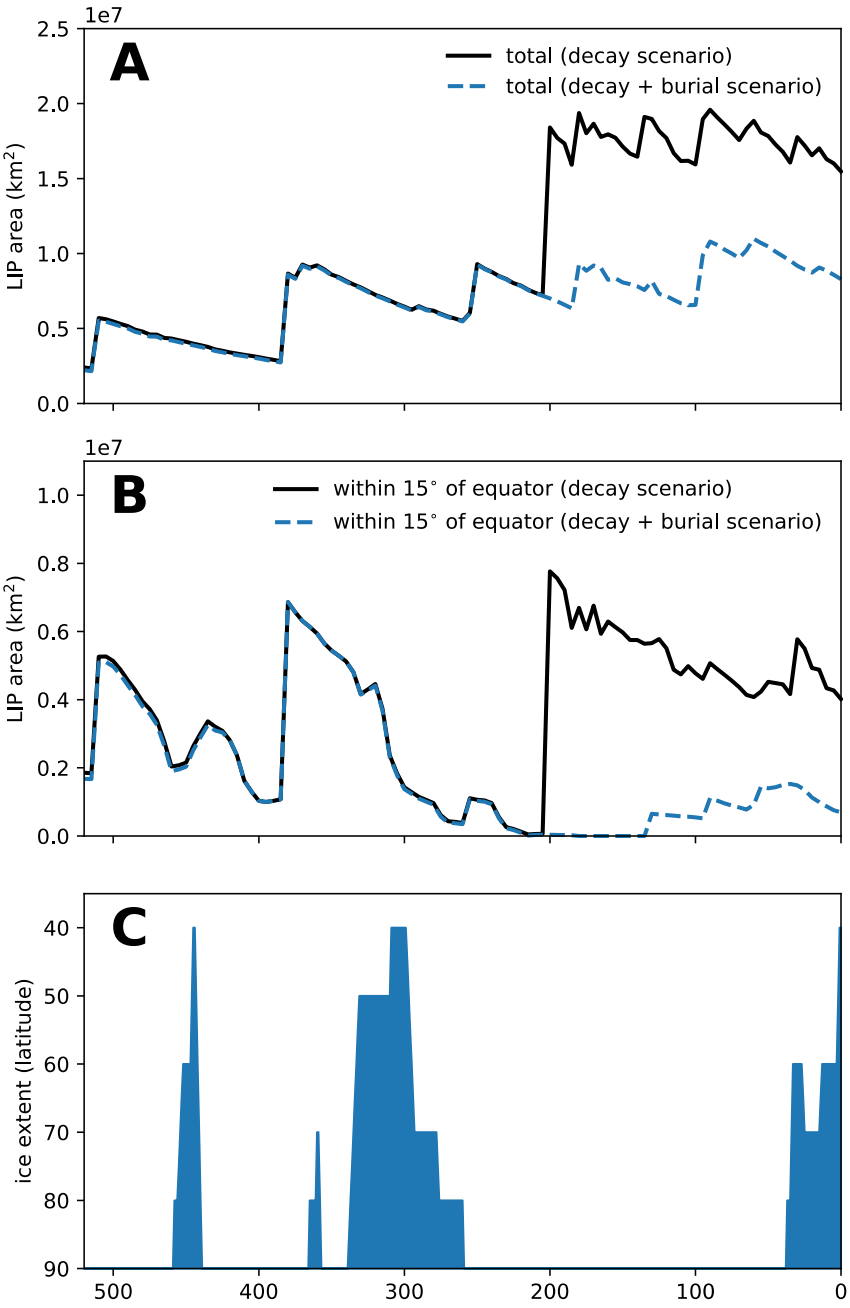

Fig. S4.

Large igneous province area in the tropics through the Phanerozoic compared to the latitudinal distribution of continental ice. A) Total area of large igneous provinces in the two different post-emplacement scenarios. B) Total area of large igneous provinces that are reconstructed to be within 15º of the equator. C) Blue marks the latitudinal extent of continental ice sheets, excluding Alpine glaciers.

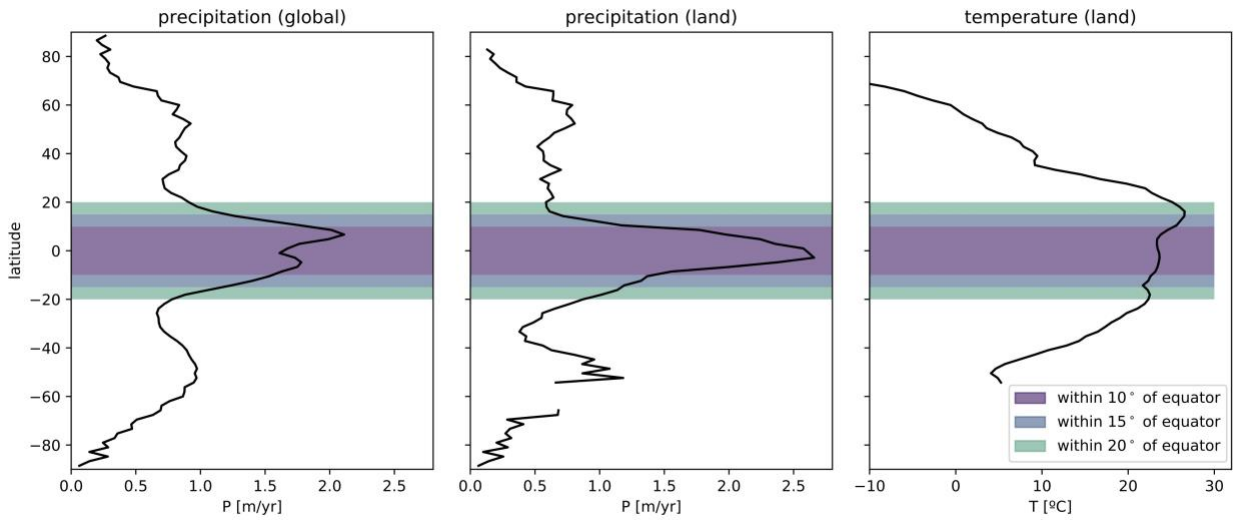

Fig. S5.

Modern climate data used to define the tropical rain belt. Zonal means of the long term monthly means from 1981 to 2010 determined through the NCEP/NCAR reanalysis 1 project (*NCEP Reanalysis data provided by the NOAA/OAR/ESRL PSD, Boulder, Colorado, USA, from their Web site at* [*https://www.esrl.noaa.gov/psd/*](https://www.esrl.noaa.gov/psd/)). The global precipitation data includes precipitation over land and oceans while the land-only precipitation data was masked to only include data over land. As a result of this masking, there is a data gap southward of ~60ºS. The latitudinal ranges used for analysis of suture length (10º, 15º and 20º from the equator) are shown for reference.

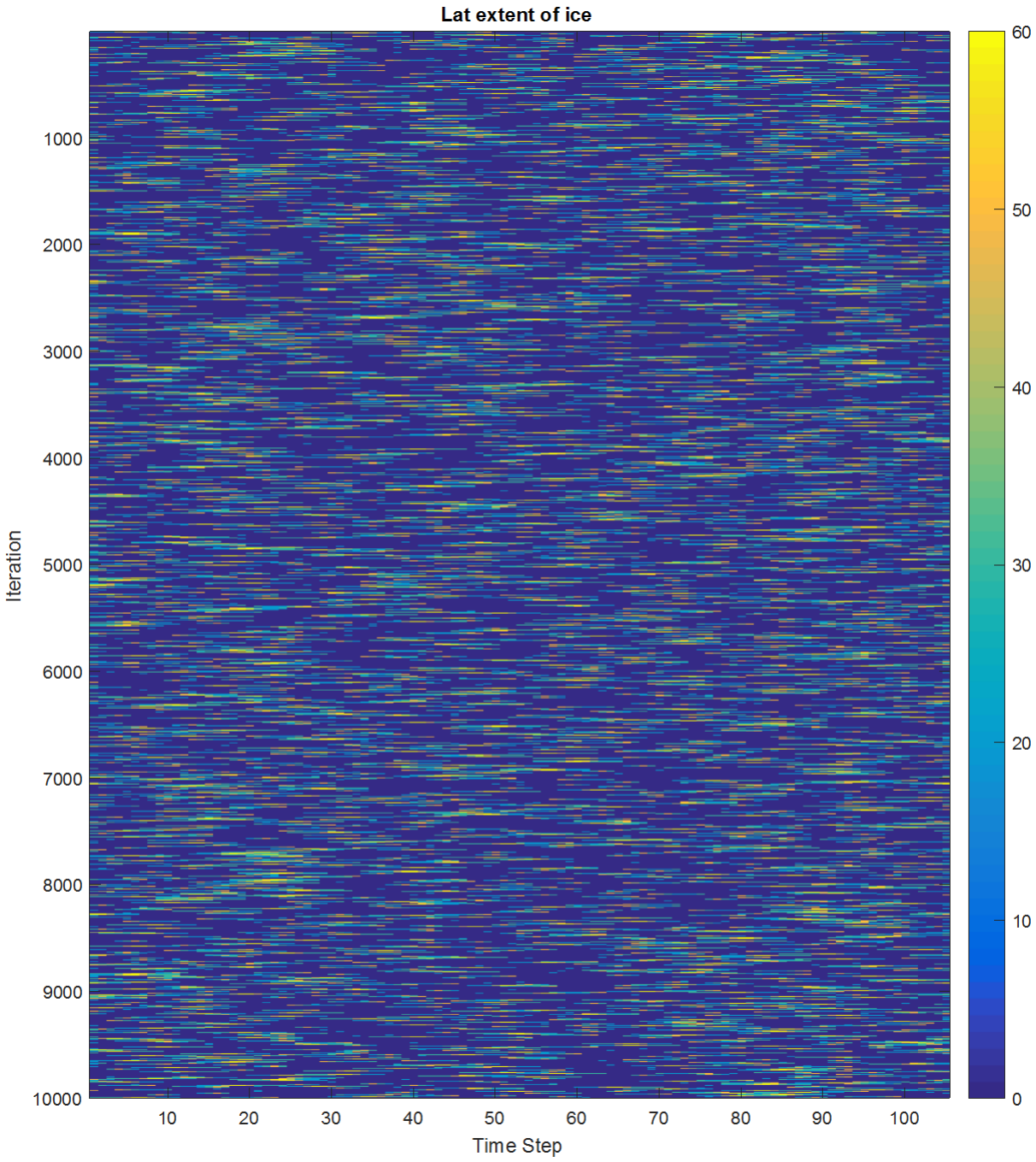

Fig. S6.

10,000 Monte Carlo simulations of the timing of glacial intervals where dark blue = no ice and yellow/orange show the max ice events. Each horizontal line represents a simulation of a glacial record through the Phanerozoic. Each time step represents 5 Myr.

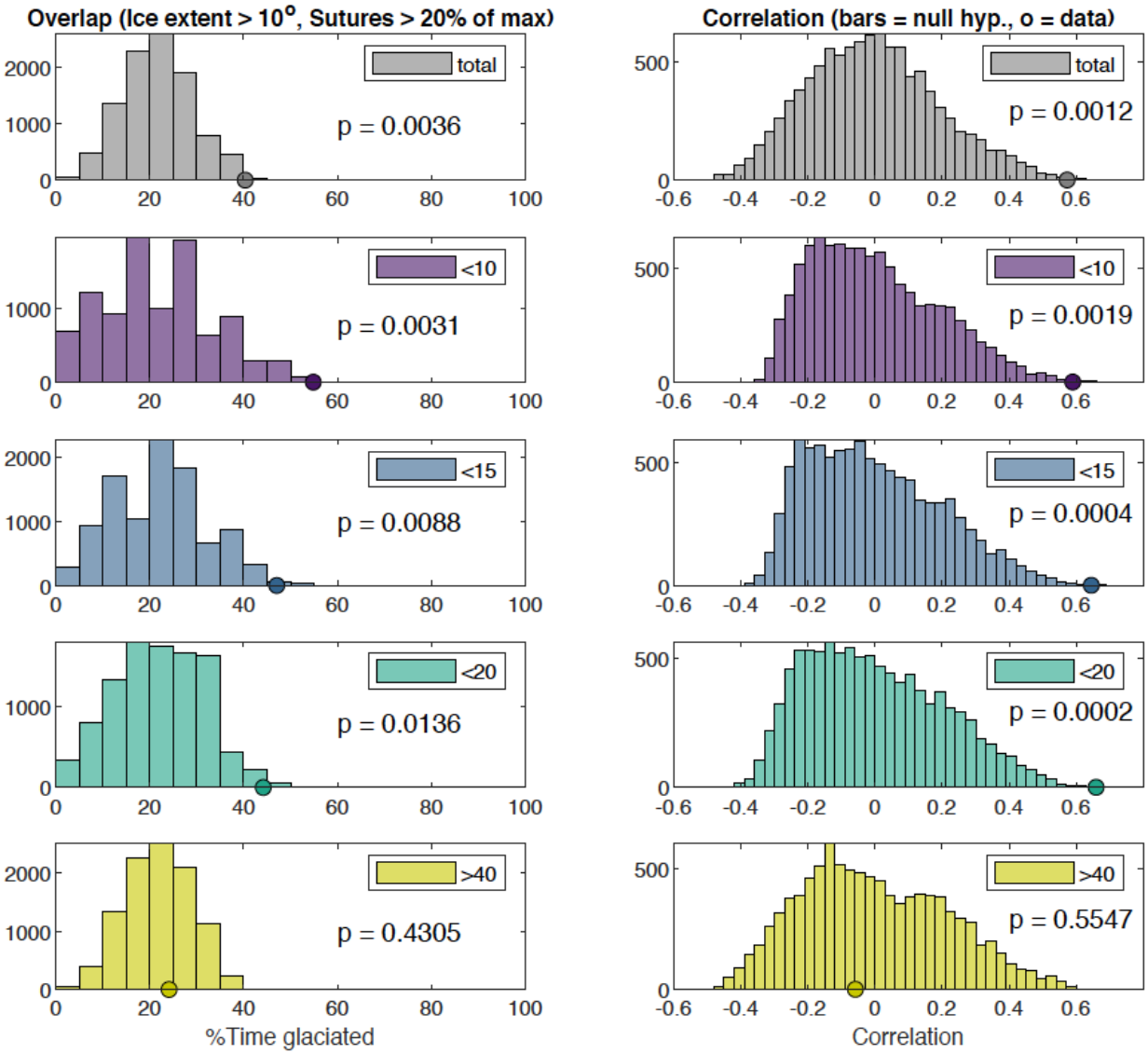

Fig. S7.

Null hypothesis of random glacial intervals compared to observed glacial intervals. Left column shows the percent of time there was significant suture length and glaciation. Significant suture length is defined as greater than 20% of the maximum, which is also the present value. Glaciation is defined as continental ice extending beyond 10º from the poles. Right column shows the correlation between sutures and ice extent for total sutures and sutures >40º, <10º, <15º, and <20º latitude. On all plots, histogram bars show the correlation coefficients obtained when comparing suture length to the random ice extent simulations, and the colored dots show the correlation coefficient obtained when comparing suture length to the observed ice extent.

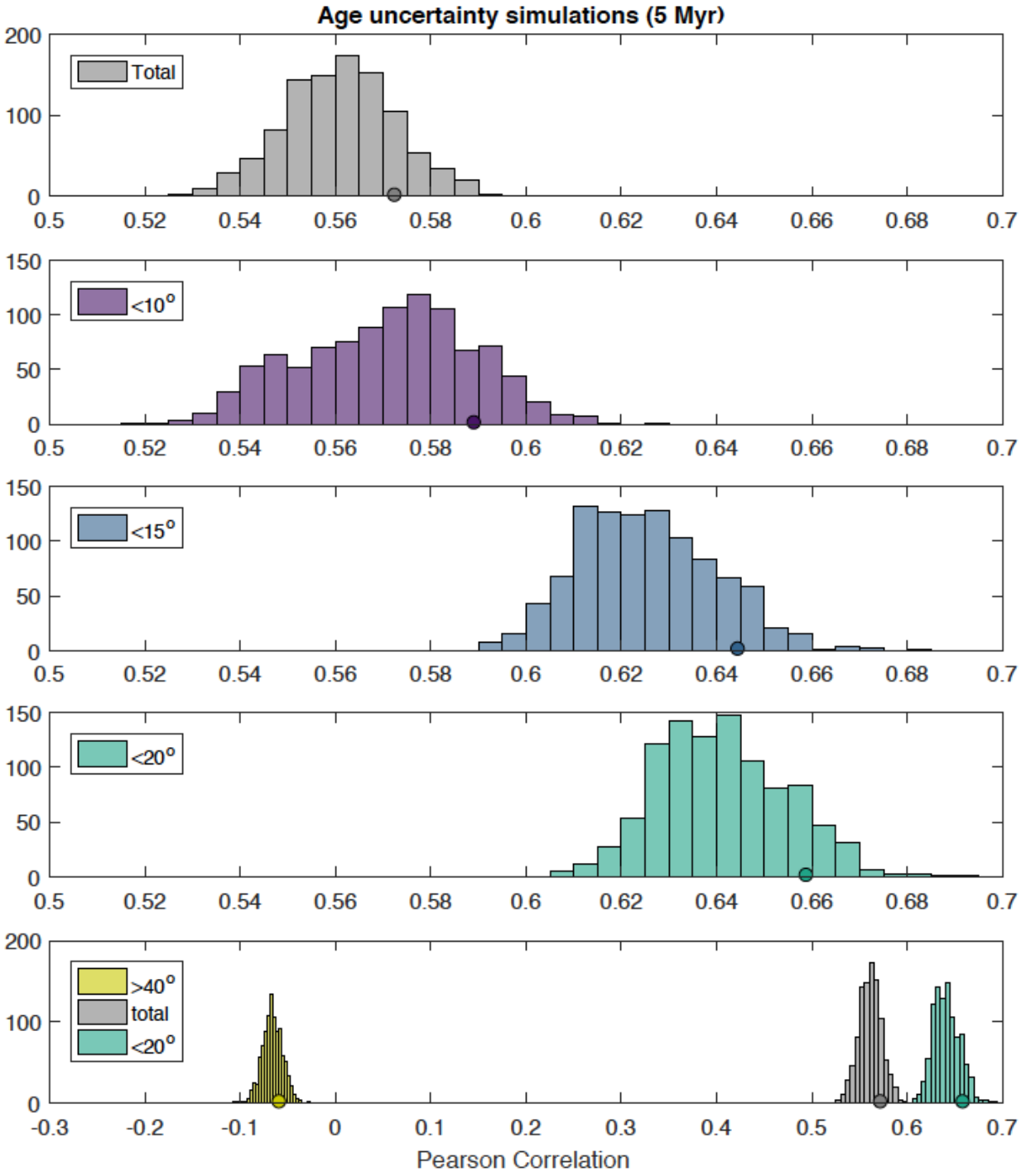

Fig. S8.

Correlation between sutures and ice extent with a simulated uncertainty in age model assuming a maximum uncertainty of 5 Myr for total sutures and sutures >40º, <10º, <15º, and <20º latitude. Histograms show the distribution of correlation coefficients with 1000 simulations applying a random walk of age uncertainty to the observed value. Filled circles are the observed correlation coefficient.

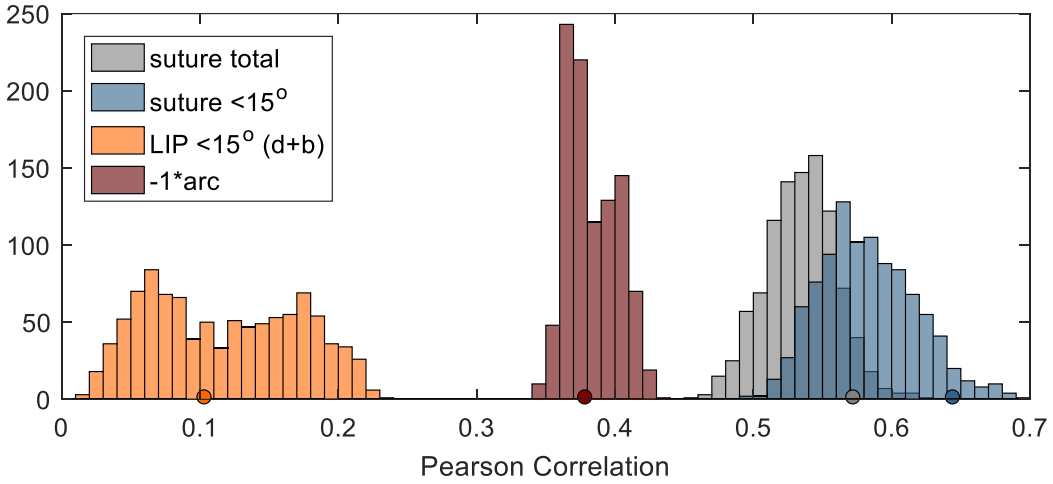

Fig. S9.
Summary of correlation between ice extent and proposed geological forcing mechanisms on climate. Histograms show the distribution of correlation in 1000 simulations of the observed values with age uncertainty simulated by a random walk scaled to a maximum of 10 Myr uncertainty. Filled circles are the observed correlation coefficient. The decay+burial scenario for large igneous provinces <15º from the tropics is in orange and the length of continental arcs of Cao et al. (32) multiplied by -1 is in maroon.

Table S1.

Suture database. Methods, data sources, and abbreviated references are described in Materials and Methods. MAGMAX and MAGMIN are minimum and maximum constraints on magmatism in the ophiolite; METMAX and METMIN are minimum and maximum constraints on metamorphism on the suture; EXMAX and EXMIN are minimum and maximum constraints on exhumation of the ophiolite; PLATE_C and PLATE_M are the plate IDs in the reconstructions of Torsvik and Cocks (*23*) and Matthews (*32*), respectively; and LENGTH is the calculated length of the suture. To fit in the table, references are given abbreviations for the first letter of the last name of the author and '+' for 'and others'.

ID	NAME	MAGMAX	MAGMIN	METMAX	METMIN	EXMAX	EXMIN	PLATE_C	PLATE_M	LENGTH	REFERENCES
1	McKlintock	510	475	480	450	465	430	134	124	435	Trettin et al. (1992)
2	Piedmont	560	460	475	450	465	440	101	101	1347	Misra & Keller (1978)
3	Moretown	560	475	475	450	465	440	101	101	1224	D+ (2008); M+ (2017)
4	Dashwoods	560	475	475	450	465	440	101	101	360	vS&B (2012); M+ (2017)
5	Amorica-Avalonia	400	380	380	370	380	360	315	315	1735	Clark et al. (1998)
6	Caledonides_Scan	498	470	475	450	465	430	302	302	1695	P&F (1991); G+ (2008)
7	Caledonides_Scot	484	470	470	464	465	440	303	315	623	Hollis et al. (2013)
8	Avalon-Gander	440	423	421	400	390	350	108	108	214	vanStaal & Barr (2012)
9	East Tasman	370	250	360	240	260	240	848	801	1637	Foster et al. (2009)
10	West Tasman	520	505	520	430	505	410	801	801	424	Foster et al. (2009)
11	Precordillera	540	470	470	359	400	359	290	202	867	R+ (2000)
12	Pampian	700	600	600	540	580	515	290	2901	1351	R+ (2000); E+ (2007)
13	S Cordilleran	270	100	120	80	100	70	291	28011	798	S+ (2008); C+ (2016)
14	N. Andean	124	72	50	40	60	0	247	201	1644	K+ (2002; 2005); M (1999)
15	Cordilleran	172	160	160	123	100	80	161	176	1628	S+ (2005); W+ (2012)
16	Anguyucham	187	184	171	160	146	90	103	18103	1366	W&B (1992); M+ (2015)
17	Windy-McKinley	376	252	360	252	265	230	16104	16104	742	M+ (2006); P+ (2018)
18	Finlayson	376	252	360	252	265	230	16104	16104	419	M+ (2006); P+ (2018)
19	N Slide Mountain	376	252	360	252	265	230	16104	16104	399	M+ (2006); P+ (2018)
20	S Slide Mountain	376	252	360	252	265	230	16104	16104	2412	B+ (1992); S+ (1991)
21	Resurrection	68	50	60	45	50	35	16121	16121	1608	H+ (2003); L+ (1997)
22	N Caribbean	124	72	106	68	70	40	233	274	1125	L+ (2009); K+ (2002)
23	W Caribbean	124	72	106	68	70	40	205	205	450	K+ (2002); M (1999)
24	S Caribbean	124	72	106	68	10	0	251	235	705	K+ (2002); M (1999)
25	Kamchatka	110	60	60	40	40	0	438	44100	593	Tsukanov et al. (2007)
26	Koryak	600	100	200	15	20	0	438	44103	991	I+ (2003)
27	NE Japan	170	150	170	0	20	0	624	624	1446	I+ (2003); Isozaki (2010)
28	Hercynian	498	390	390	330	335	300	305	305	3654	K&R (2013); H&O (2001)
29	Magnitogorsk	488	392	416	375	375	358	302	302	2653	Brown et al. (2006)
30	Sananadaj-Sirjan	97	90	90	72	90	72	503	503	3556	M&S (2015); S&S (2014)
31	Semail	97	90	90	72	90	72	503	503	677	R+ (2016); S&S (2014)
32	Pontides	165	120	153	50	70	35	581	521	1829	O&T (1999); B+ (2013)
33	Shyok	120	40	120	0	40	0	563	517	2065	Bouilhol et al. (2013)
34	Indus-Tsangpo	165	120	153	50	50	0	501	501	2698	J+ (2015); H+. (2012)
35	Quetta	80	65	65	35	66	49	501	501	1279	Beck et al. (1995)
36	WestJinsha	290	258	230	190	230	195	616	616	1110	Schwab et al. (2004)
37	Bangong	471	244	244	135	90	78	616	606	2321	Z+ (2011); Z+ (2012)
38	NW Kunlun	474	458	451	384	250	210	456	456	1190	S+ (2004); X+ (2002)
39	Jinsha	290	258	230	190	230	195	616	616	1998	S+ (2004); Y+ (2012)
40	Ailaoshan	387	341	341	247	247	237	602	602	1102	Z+ (2012); M (2013)
41	Cheng-Menglian	386	264	264	250	250	235	603	60301	1557	J+ (2009); M (2013)
42	Kunlun	474	244	451	384	250	210	456	456	1714	S+. (2004); X+ (2002)
43	Tianshan-Tarim	397	387	387	361	360	330	451	451	1580	Wang et al. (2011)
44	Erementay-Yili	530	460	443	413	443	413	1019	460	338	Domeier (2018)
45	Junggar-Balkhash	490	344	344	316	316	270	461	464	657	Han et al. (2010)
46	Maikain-Kyzyltas	503	460	460	440	458	419	1021	462	674	Choulet et al. (2012)
47	Central Asian	360	250	330	250	250	240	453	453	1881	Xiao et al. (2015)
48	Transaltai	415	390	390	360	360	300	455	455	2319	Kroner et al. (2010)
49	Khantaishir	580	550	550	540	540	530	432	432	1554	Bold et al. (2016)
50	Bayankhongor	653	651	650	200	160	140	432	401	398	B+ (2001); D+ (2013)

51	Derba_Olkhon	579	480	490	430	490	430	401	401	1089	D&B (2007); C+ (2015)
52	Kurtushiba	470	465	470	430	470	430	431	431	304	Volkova et al. (2011)
53	Uralian	488	392	416	275	315	265	302	302	3191	Brown et al. (2006)
54	Mongol-Okhotsk	380	200	250	150	160	140	430	430	2775	Donskaya et al. (2013)
55	Dabie-Sulu	488	470	470	440	250	210	601	601	1015	R+ (2004)
56	Primorye	622	430	330	220	250	210	454	454	1321	I&T (2003)
57	Japan	600	280	330	220	250	210	630	630	891	I&T (2003)
58	Banda	83	3	36	0	5	0	683	652	573	Harris (2006)
59	Java	198	100	90	66	8	0	673	736	713	Wakita (2000)
60	NewGuinea	190	56	58	15	15	0	680	698	1996	B+ (2012); C+ (2005)
61	Cyclops	43	29	29	16	4	0	697	697	310	Monnier et al. (1999a)
62	Seram	20	10	16	6	6	0	681	681	228	M+ (2003); P+ (2016)
63	Obi	116	60	60	35	4	0	670	567	101	Ali et al. (2001)
64	Halmahera	165	66	66	35	4	0	680	680	595	H+ (1988); B (1996)
65	EastSulawesi	60	40	34	23	23	0	667	667	905	P (1988); V+ (2002)
66	Borneo_Palawan	198	76	100	11	23	0	677	61405	1958	M+ (1999b); D&B (1996)
67	EastPhilippines	180	23	107	11	20	0	678	678	1761	P+ (1991); Y+ (2007)
68	WestPhilippines	160	23	48	11	5	0	674	674	717	Y+ (2009;2013)
75	Verkhoyansk	430	180	180	135	146	90	420	420	872	Osman (2003)
78	WestAlpine	200	100	50	30	50	30	304	304	3236	Michard et al. (2002)
79	Maghebrides	40	20	23	10	23	0	706	718	3371	M+ (2002); AV+ (2014)
80	Bentong-Raub	400	300	300	250	250	235	647	647	418	Metcalfe (2013)
81	MtVictoria-Kawlun	165	120	153	50	39	0	607	607	1279	Burchfiel et al. (2012)
82	Woyla	95	48	90	48	60	40	647	647	2636	Pedersen et al. (2010)
83	Mahkran	165	120	153	72	90	72	582	50602	489	M&S (2015); T+ (1983)
84	Sistan	114	85	85	65	83	65	506	505	754	B+ (2013); T+ (1983)
85	Alborz	599	522	382	330	299	250	392	301	2733	M&S (2014)
87	South_Anyui1	187	184	171	160	146	90	407	43300	450	Moore et al. (2015)
88	South_Anyui2	187	184	171	160	146	90	407	43300	1091	Moore et al. (2015)
89	Hispaniola	124	72	106	68	10	0	240	254	846	Mann (1999)
90	Avalon_Meritimes	440	223	421	400	421	400	108	108	605	van Staal & Barr (2012)
91	Avalon_NE	440	423	421	400	421	400	108	108	182	van Staal & Barr (2012)
92	Meguma	400	380	400	380	390	350	170	108	879	van Staal & Barr (2012)
93	Maurintanides	498	390	390	330	335	295	714	714	812	P&M (1989); V (2005)
94	Avalon_Britian	440	423	421	400	421	400	315	315	566	Pharroah (1999)
95	Caledonides_Green	498	470	475	430	465	430	102	102	1245	Gee et al. (2008)
96	Caledonides_Sval	498	470	475	430	465	430	309	309	282	Gee et al. (2008)
97	Kudi-Altyn	526	458	490	444	475	444	480	580	1326	X+ (2002); L+ (2016)
98	Pie de Palo	1090	1027	1030	475	475	444	290	202	276	Ramos et al. (2000)
99	Ogcheon	480	430	430	330	430	330	601	601	383	Cluzel (1992)
100	Shan States	250	155	155	120	155	120	607	7250	1098	Metcalfe (2013)
103	Slonoker	360	250	330	250	250	240	401	401	1019	Xiao et al. (2015)
104	Anarek-Dehshir	97	90	90	72	90	72	582	505	1020	M&S (2015)
105	Zagros	90	65	70	0	10	0	582	505	2500	Alavi (1994)
106	Inner Taurus	90	65	70	0	10	0	504	522	850	Alavi (1994)
107	Tuarkyr	360	310	340	290	330	300	302	302	2258	G&G (2002)
108	New Caledonia	220	50	60	34	44	33	806	845	591	Cluzel et al. (2012)
109	Tangihua	220	50	60	34	44	33	806	806	298	N+ (2000)
110	Dun_North	285	265	160	100	130	90	806	806	151	S&M(2010); G&F(2004)
111	Dun_South	285	265	160	100	130	90	806	806	159	S&M (2010)
112	Northland	35	15	26	20	23	15	806	806	205	W+ (2006); M+ (2014)
113	Caltepec	480	275	350	320	335	295	215	215	1019	N+ (2010); G+ (1995)
114	Alleghenian	390	300	390	295	335	295	109	109	1169	Nance et al. (2010)
115	Qilian	540	500	473	446	446	420	601	601	2074	Song et al. (2014)
116	Kyrgyz M Tianshan	467	445	460	450	458	444	1019	1019	732	Alexeiev et al. (2016)
117	Kyrgyz N Tianshan	534	508	508	474	485	470	1019	1019	1016	A+ (2011); D (2018)

Table S2.

Large igneous province database. Methods and data sources described in Materials and Methods.

ID	NAME	AGE	PLATEID	AREA (Mkm2)	SUM AREA (Mkm2)	BURIED (Y/N)
L1	Columbia River	16	101	0.676	0.676	N
L2a	Afar	30	503	1.417	2.047	Y
L2b	Afar	30	715	0.63		Y
L3a	NAIP	62	102	0.253	1.072	Y
L3b	NAIP	62	303	0.819		Y
L4	Deccan	66	501	0.831	0.831	N
L5	Seychelles	66	501	0.456	0.456	Y
L6	Madagascar	90	702	0.627	0.627	N
L7a	Caribbean-Colombian	94	246	0.031	0.712	N
L7b	Caribbean-Colombian	94	247	0.009		N
L7c	Caribbean-Colombian	94	244	0.006		N
L7d	Caribbean-Colombian	94	237	0.248		N
L7e	Caribbean-Colombian	94	245	0.005		N
L7f	Caribbean-Colombian	94	243	0.047		N
L7g	Caribbean-Colombian	94	240	0.057		N
L7h	Caribbean-Colombian	94	204	0.135		N
L7i	Caribbean-Colombian	94	239	0.001		N
L7j	Caribbean-Colombian	94	249	0.006		N
L7k	Caribbean-Colombian	94	248	0.061		N
L7l	Caribbean-Colombian	94	248	0.108		N
L8a	HALIP	95	120	0.919	3.597	N
L8b	HALIP	95	102	0.025		N
L8c	HALIP	95	121	0.187		N
L8d	HALIP	95	415	2.053		N
L8e	HALIP	95	415	0.362		N
L8f	HALIP	95	311	0.051		N
L9	EQUAMP	131	201	0.66	0.66	N
L10	Comei	132	606	0.032	0.032	N
L11	Bunbury	132	801	0.105	0.105	N
L12a	Parana-Etendeka	135	202	0.022	3.121	Y
L12b	Parana-Etendeka	135	201	0.873		Y
L12c	Parana-Etendeka	135	701	1.577		Y
L12d	Parana-Etendeka	135	701	0.564		Y
L12e	Parana-Etendeka	135	290	0.085		Y
L13	Trap	140	102	0.03	0.03	N
L14	NW Australia Margin	160	801	0.619	0.619	Y
L15	Karoo	183	701	3.207	3.207	N
L16a	Ferrar	183	841	0.091	0.179	N
L16b	Ferrar	183	841	0.062		N
L16c	Ferrar	183	841	0.025		N
L17a	CAMP	201	714	4.39	11.457	Y
L17b	CAMP	201	101	5.495		Y
L17c	CAMP	201	201	1.339		Y
L17d	CAMP	201	305	0.219		Y
L17e	CAMP	201	304	0.014		Y
L18	Siberia	252	401	3.459	3.459	N
L19	Emeishan	259	602	0.706	0.706	N
L20	Panjal	283	563	0.066	0.066	N
L21	Qiangtang	283	616	0.045	0.045	N
L22a	Tarim	290	480	0.156	0.355	N
L22b	Tarim	290	480	0.199		N
L23	Magdalen	360	101	0.422	0.422	N
L24	Vilyui	374	404	1.144	1.144	N
L25	Kola-Dnieper	380	302	5.899	5.899	N
L26	Suordakh	450	420	0.018	0.018	N
L27	Kalkarindji	511	801	3.544	3.544	N

Table S3.
Phanerozoic ice extent. Methods and data sources are described in Materials and Methods.

AGE	LAT	GLACIATED REGION	REFERENCE	AGE	LAT	GLACIATED REGION	REFERENCE
0	50	USA Midwest	Ehlers & Gibbard (2007)	263	10	SE Australia	M&P (2013); F+ (2008)
1	50	USA Midwest	Ehlers & Gibbard (2007)	264	10	SE Australia	M&P (2013); F+ (2008)
2	40	Canada	Ehlers & Gibbard (2007)	265	10	SE Australia	M&P (2013); F+ (2008)
3	30	Greenland	Ehlers & Gibbard (2007)	266	10	SE Australia	M&P (2013); F+ (2008)
4	30	Greenland	Ehlers & Gibbard (2007)	267	10	SE Australia	M&P (2013); F+ (2008)
5	30	Greenand	Ehlers & Gibbard (2007)	268	10	SE Australia	M&P (2013); F+ (2008)
6	30	Antarctic Peninsula	Ehlers & Gibbard (2007)	269	10	SE Australia	M&P (2013); F+ (2008)
7	30	Antarctic Peninsula	Ehlers & Gibbard (2007)	270	10	SE Australia	M&P (2013); F+ (2008)
8	30	Antarctic Peninsula	Ehlers & Gibbard (2007)	271	10	SE Australia	M&P (2013); F+ (2008)
9	30	Antarctic Peninsula	Ehlers & Gibbard (2007)	272	10	SE Australia	M&P (2013); F+ (2008)
10	30	Antarctic Peninsula	Ehlers & Gibbard (2007)	273	10	SE Australia	M&P (2013); F+ (2008)
11	30	Antarctic Peninsula	Ehlers & Gibbard (2007)	274	10	SE Australia	M&P (2013); F+ (2008)
12	30	Antarctic Peninsula	Ehlers & Gibbard (2007)	275	10	SE Australia	M&P (2013); F+ (2008)
13	30	Antarctic Peninsula	Ehlers & Gibbard (2007)	276	10	SE Australia	M&P (2013); F+ (2008)
14	25	Antarctica	D&L (1998); T & R (2002)	277	15	W Australia	M&P (2013); F+ (2008)
15	20	Antarctica	D&L (1998); T & R (2002)	278	20	W Australia	M&P (2013); F+ (2008)
16	20	Antarctica	D&L (1998); T & R (2002)	279	20	W Australia	M&P (2013); F+ (2008)
17	20	Antarctica	D&L (1998); T & R (2002)	280	20	W Australia	M&P (2013); F+ (2008)
18	20	Antarctica	D&L (1998); T & R (2002)	281	20	W Australia	M&P (2013); F+ (2008)
19	20	Antarctica	D&L (1998); T & R (2002)	282	20	W Australia	M&P (2013); F+ (2008)
20	20	Antarctica	D&L (1998); T & R (2002)	283	20	W Australia	M&P (2013); F+ (2008)
21	20	Antarctica	D&L (1998); T & R (2002)	284	20	W Australia	M&P (2013); F+ (2008)
22	20	Antarctica	D&L (1998); T & R (2002)	285	20	W Australia	M&P (2013); F+ (2008)
23	20	Antarctica	D&L (1998); T & R (2002)	286	20	W Australia	M&P (2013); F+ (2008)
24	20	Antarctica	D&L (1998); T & R (2002)	287	20	W Australia	M&P (2013); F+ (2008)
25	20	Antarctica	D&L (1998); T & R (2002)	288	20	W Australia	M&P (2013); F+ (2008)
26	25	Antarctica	D&L (1998); T & R (2002)	289	20	W Australia	M&P (2013); F+ (2008)
27	30	Antarctic Peninsula	Ivany et al. (2006)	290	20	W Australia	M&P (2013); F+ (2008)
28	30	Antarctic Peninsula	Ivany et al. (2006)	291	20	W Australia	M&P (2013); F+ (2008)
29	30	Antarctic Peninsula	Ivany et al. (2006)	292	20	W Australia	M&P (2013); F+ (2008)
30	30	Antarctic Peninsula	Ivany et al. (2006)	293	20	W Australia	M&P (2013); F+ (2008)
31	30	Antarctic Peninsula	Ivany et al. (2006)	294	25	Australia	M&P (2013); F+ (2008)
32	30	Antarctic Peninsula	Ivany et al. (2006)	295	30	Australia	M&P (2013); F+ (2008)
33	30	Antarctic Peninsula	Ivany et al. (2006)	296	35	Australia	M&P (2013); F+ (2008)
34	20	Antarctica	Z+ (2001); DB+ (2010)	297	40	Australia	M&P (2013); F+ (2008)
35	10	Antarctica	Z+ (2001); DB+ (2010)	298	45	Australia	M&P (2013); F+ (2008)
36	10	Antarctica	Z+ (2001); DB+ (2010)	299	50	Brazil,Arabia,Africa	M&P (2013); T&C (2013)
37	10	Antarctica	Z+ (2001); DB+ (2010)	300	50	Brazil,Arabia,Africa	M&P (2013); T&C (2013)
38-259	0	-	Crowley (1988)	301	50	Brazil,Arabia,Africa	M&P (2013); T&C (2013)
260	10	SE Australia	M&P (2013); F+ (2008)	302	50	Brazil,Arabia,Africa	M&P (2013); T&C (2013)
261	10	SE Australia	M&P (2013); F+ (2008)	303	50	Brazil,Arabia,Africa	M&P (2013); T&C (2013)
262	10	SE Australia	M&P (2013); F+ (2008)	304	50	Brazil,Arabia,Africa	M&P (2013); T&C (2013)

AGE	LAT	GLACIATED REGION	REFERENCE
305	50	Brazil,Arabia,Africa	M&P (2013); T&C (2013)
306	50	Brazil,Arabia,Africa	M&P (2013); T&C (2013)
307	50	Brazil,Arabia,Africa	M&P (2013); T&C (2013)
308	50	Brazil,Arabia,Africa	M&P (2013); T&C (2013)
309	50	Brazil,Arabia,Africa	M&P (2013); T&C (2013)
310	40	E Australia	V&P (1987)
311	40	E Australia	V&P (1987)
312	40	E Australia	V&P (1987)
313	40	E Australia	V&P (1987)
314	40	E Australia	V&P (1987)
315	40	E Australia	V&P (1987)
316	40	E Australia	V&P (1987)
317	40	E Australia	V&P (1987)
318	40	E Australia	V&P (1987)
319	40	E Australia	V&P (1987)
320	40	E Australia	V&P (1987)
321	40	E Australia	V&P (1987)
322	40	E Australia	V&P (1987)
323	40	E Australia	V&P (1987)
324	40	E Australia	V&P (1987)
325	40	E Australia	V&P (1987)
326	40	E Australia	V&P (1987)
327	40	E Australia	V&P (1987)
328	40	E Australia	V&P (1987)
329	40	E Australia	V&P (1987)
330	40	E Australia	V&P (1987)
331	40	E Australia	V&P (1987)
332	35	S Africa & S Am (?)	M&P (2013); F+ (2008)
333	30	S Africa & S Am (?)	M&P (2013); F+ (2008)
334	25	S Africa & S Am (?)	M&P (2013); F+ (2008)
335	20	S Africa & S Am (?)	M&P (2013); F+ (2008)
336	15	S Africa & S Am (?)	M&P (2013); F+ (2008)
337	10	S Africa & S Am (?)	M&P (2013); F+ (2008)
338	5	S Africa & S Am (?)	M&P (2013); F+ (2008)
339-357	0	-	Crowley (1988)
358	10	Brazil, C Africa (?)	Isaacson et al. (2008)
359	20	S Am, C Africa	Isaacson et al. (2008)
360	20	S Am, C Africa	Isaacson et al. (2008)
361	10	Brazil, C Africa (?)	Isaacson et al. (2008)
362	10	Brazil, C Africa (?)	Isaacson et al. (2008)
363	10	Brazil, C Africa (?)	Isaacson et al. (2008)
364	10	Brazil, C Africa (?)	Isaacson et al. (2008)
365	10	Brazil, C Africa (?)	Isaacson et al. (2008)
366-439	0	-	Crowley (1988)
440	10	S America	DM+ (2007)
441	20	S America	DM+ (2007)
442	30	S America	DM+ (2007)
443	40	S America	DM+ (2007)
444	50	Arabia	DM+ (2007)
445	50	Arabia	DM+ (2007)
446	40	Peri-Gond, N Africa	Hambrey (1985)
447	30	Peri-Gond, N Africa	Hambrey (1985)
448	30	Peri-Gond, N Africa	Hambrey (1985)
449	30	Peri-Gond, N Africa	Hambrey (1985)
450	30	Peri-Gond, N Africa	Hambrey (1985)
451	30	Peri-Gond, N Africa	Hambrey (1985)
452	30	Peri-Gond, N Africa	Hambrey (1985)
453	25	Peri-Gond, N Africa	Hambrey (1985)
454	20	Morocco	Saltzmann et al. (2005)
455	15	Morocco	Saltzmann et al. (2005)
456	10	Morocco	Saltzmann et al. (2005)
457	10	Morocco	Saltzmann et al. (2005)
458	10	Morocco	Saltzmann et al. (2005)
459-520	0	-	Crowley (1988)

Table S4.
Correlation statistics for ice extent and overlap of glacial record with suture length, large igneous provinces,and arc length, including p-values with respect to the null-hypothesis. Methods are described in Materials and Methods.

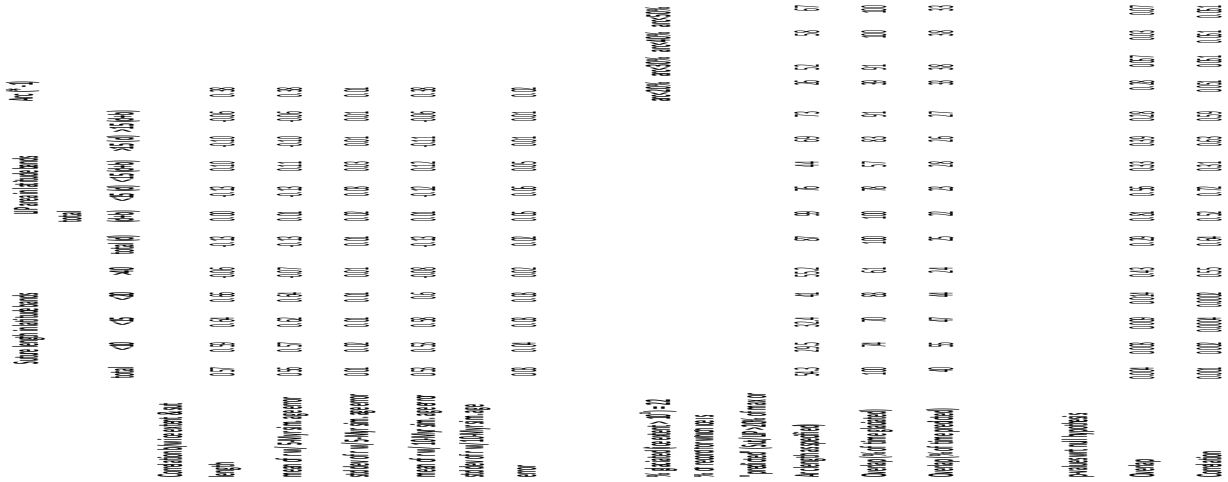

Movie S1.
Five-million year snapshots of paleogeographic reconstruction of active sutures from 520 Ma to present. Continental outlines shown are the tectonic units of Torsvik and Cocks (*23*). Green band is 15° above and below the equator. Blue shade is ice-extent from database (Table S3). For simplicity and visualization ice-extent is shown as uniform along a given longitude, where in reality there were regional differences. Methods described in Materials and Methods section.

References and Notes

31. J. Hartmann, N. Moosdorf, *Geochemistry, Geophysics, Geosystems* **13**, (2012).
32. K. J. Matthews *et al.*, *Global and Planetary Change* **146**, 226-250 (2016).
33. Y. Dilek, H. Furnes, *Geological Society of America Bulletin* **123**, 387-411 (2011).
34. Y. Dilek, H. Furnes, *Elements* **10**, 93-100 (2014).
35. C. R. van Staal *et al.*, **40**, 94-117 (2013).
36. F. A. Macdonald *et al.*, *American Journal of Science* **317**, 555-596 (2017).
37. M. Rioux *et al.*, *Earth and Planetary Science Letters* **451**, 185-195 (2016).
38. K. Burke, J. Dewey, W. Kidd, *Tectonophysics* **40**, 69-99 (1977).
39. H. Furnes, M. De Wit, Y. Dilek, *Geoscience Frontiers* **5**, 571-603 (2014).
40. A. C. Sengor, B. A. Natal'in, in *The Tectonic Evolution of Asia*, A. Yin, M. Harrison, Eds. (Cambridge University Press, Cambridge, 1996), pp. 486-640.
41. R. Hall, *Annual Review of Earth and Planetary Sciences* **45**, 331-358 (2017).
42. K. Wakita, *Journal of Asian Earth Sciences* **18**, 739-749 (2000).
43. C. Monnier *et al.*, *Geodinamica Acta* **12**, 43-55 (1999).
44. G. P. Yumul Jr, C. B. Dimalanta, E. J. Marquez, K. L. Queaño, *Journal of Asian Earth Sciences* **34**, 610-623 (2009).
45. J. Coggon, G. Nowell, D. Pearson, S. Parman, *Economic Geology* **106**, 93-117 (2011).
46. J. Encarnacion, E. Essene, S. Mukasa, C. Hall, *Journal of Petrology* **36**, 1481-1503 (1995).
47. D. Witts, R. Hall, G. Nichols, R. Morley, *Journal of Asian Earth Sciences* **56**, 77-104 (2012).
48. R. Hall, *Journal of Asian Earth Sciences* **20**, 353-431 (2002).
49. C. Parkinson, *Journal of Asian Earth Sciences* **16**, 13-28 (1998).
50. J. Hennig, R. Hall, M. A. Forster, B. P. Kohn, G. S. Lister, *Tectonophysics* **712**, 600-622 (2017).
51. S. C. Bergman, D. Q. Coffield, J. P. Talbot, R. A. Garrard, *Geological Society, London, Special Publications* **106**, 391-429 (1996).
52. A. Q. van Ufford, M. Cloos, *AAPG bulletin* **89**, 119-140 (2005).
53. S. L. Baldwin, P. G. Fitzgerald, L. E. Webb, *Annual Review of Earth and Planetary Sciences* **40**, 495-520 (2012).
54. W. B. Hamilton, *Tectonics of the Indonesian region*. (US Govt. Print. Off., 1979).
55. M. Cloos *et al.*, *Geological Society of America Special Papers* **400**, 1-51 (2005).
56. H. L. Davies, I. E. Smith, *Geological Society of America Bulletin* **82**, 3299-3312 (1971).
57. H. Davies, A. Jaques, *Geological Society, London, Special Publications* **13**, 341-349 (1984).
58. J. Ali, R. Hall, S. Baker, *Journal of Asian Earth Sciences* **19**, 535-546 (2001).
59. R. Hall, M. Audley-Charles, F. Banner, S. Hidayat, S. Tobing, *Journal of the Geological Society* **145**, 65-84 (1988).
60. P. Ballantyne, *Geological Society, London, Special Publications* **60**, 179-202 (1992).
61. C. Monnier *et al.*, *Mineralogy and Petrology* **65**, 1-28 (1999).
62. G. P. Yumul, *Island Arc* **16**, 306-317 (2007).
63. M. Pubellier *et al.*, *Journal of Southeast Asian Earth Sciences* **6**, 239-248 (1991).
64. G. P. Yumul Jr, C. B. Dimalanta, R. A. Tamayo Jr, D. V. Faustino-Eslava, *Journal of Asian Earth Sciences* **65**, 53-63 (2013).

65. R. Harris, *Gondwana Research* **10**, 207-231 (2006).
66. J. M. Pownall, M. A. Forster, R. Hall, I. M. Watkinson, *Gondwana Research* **44**, 35-53 (2017).
67. C. Monnier *et al.*, *Bulletin de la Société géologique de France* **174**, 529-543 (2003).
68. D. Cluzel, F. Jourdan, S. Meffre, P. Maurizot, S. J. T. Lesimple, *Tectonics* **31**, 1-18 (2012).
69. D. N. Reusch, *Geology* **39**, 807-810 (2011).
70. K. Nicholson, P. Black, C. J. T. Picard, **321**, 1-15 (2000).
71. S. A. Whattam, J. Malpas, I. E. Smith, J. R. J. E. Ali, P. S. Letters, **250**, 606-632 (2006).
72. K. Marsaglia *et al.*, **57**, 219-235 (2014).
73. W. Sivell, M. J. N. Z. J. o. G. McCulloch, Geophysics, **43**, 133-146 (2000).
74. D. Gray, D. J. T. Foster, **385**, 181-210 (2004).
75. A. Parsons *et al.*, *Geological Socety of America Bulletin* **131**, 274-298 (2018).
76. M. Colpron, J. L. Nelson, D. C. Murphy, *GSA Today* **17**, 1-7 (2007).
77. B. C. Burchfiel, D. S. Cowan, G. A. Davis, in *The Geology of North America*, B. C. Burchfield, P. W. Lipman, M. L. Zoback, Eds. (Geological Society of America, Boulder, 1992), vol. G-3, The Cordilleran Orogen: Conterminous U.S., chap. 8, pp. 407-479.
78. D. C. Murphy *et al.*, *Geological Association of Canada Special Paper* **45**, 75-105 (2006).
79. J. K. Snow, Y. Asmerom, D. R. Lux, *Geology* **19**, 629-632 (1991).
80. G. L. Farmer, D. J. J. J. o. G. R. S. E. DePaolo, **88**, 3379-3401 (1983).
81. J. W. Shervais, B. L. Murchey, D. L. Kimbrough, P. R. Renne, B. Hanan, *Geological Society of America Bulletin* **117**, 633-653 (2005).
82. J. Wakabayashi, *Tectonophysics* **568**, 230-247 (2012).
83. W. R. Dickinson, E. I. J. G. S. o. A. B. Rich, **83**, 3007-3024 (1972).
84. J. S. Pallister, J. R. Budahn, B. L. Murchey, *Journal of Geophysical Research: Solid Earth* **94**, 15901-15923 (1989).
85. R. Harris, *Geological Society, London, Special Publications* **60**, 301-325 (1992).
86. K. R. Wirth, J. M. Bird, *Geology* **20**, 75-78 (1992).
87. T. E. Moore, P. B. O'Sullivan, C. J. Potter, R. A. Donelick, *Geosphere* **11**, 93-122 (2015).
88. J. Lytwyn, J. Casey, S. Gilbert, T. Kusky, *Journal of Geophysical Research: Solid Earth* **102**, 10225-10243 (1997).
89. P. J. Haeussler, D. C. Bradley, R. E. Wells, M. L. Miller, *Geological Society of America Bulletin* **115**, 867-880 (2003).
90. Y. Isozaki, K. Aoki, T. Nakama, S. Yanai, *Gondwana Research* **18**, 82-105 (2010).
91. A. Ishiwatari, S. D. Sokolov, S. V. Vysotskiy, *Geological Society, London, Special Publications* **218**, 597-617 (2003).
92. N. V. Tsukanov, W. Kramer, S. G. Skolotnev, M. V. Luchitskaya, W. Seifert, *island Arc* **16**, 431-456 (2007).
93. J. Escuder-Viruete, A. Pérez-Estaun, M. Joubert, D. Weis, *Geologica Acta* **9**, (2011).
94. A. C. Kerr *et al.*, *Journal of Geophysical Research: Solid Earth* **107**, (2002).
95. A. C. Kerr, J. Tarney, *Geology* **33**, 269-272 (2005).
96. C. Lázaro *et al.*, *Journal of Metamorphic Geology* **27**, 19-40 (2009).
97. P. Mann, in *Sedimentary Basins of the World*. (Elsevier, 1999), vol. 4, pp. 3-31.
98. F. Sepúlveda, F. Hervé, M. Calderón, J. Lacassie, *Gondwana Research* **13**, 238-249 (2008).

99. M. Calderón *et al.*, in *Geodynamic Evolution of the Southernmost Andes*. (Springer, 2016), pp. 7-36.
100. G. M. Stampfli, G. Borel, *Earth and Planetary Science Letters* **196**, 17-33 (2002).
101. A. C. Şengör, J. Stock, *Geoscience Canada* **41**, 225-254 (2014).
102. H. S. Moghadam, R. J. Stern, *Journal of Asian Earth Sciences* **100**, 31-59 (2015).
103. R. Tirrul, I. Bell, R. Griffis, V. Camp, *Geological Society of America Bulletin* **94**, 134-150 (1983).
104. A. Michard, A. Chalouan, H. Feinberg, B. Goffé, R. Montigny, *Bulletin de la Société géologique de France* **173**, 3-15 (2002).
105. E. Bozkurt, J. A. Winchester, M. Satır, *Tectonophysics* **595**, 198-214 (2013).
106. A. I. Okay, O. Tüysüz, *Geological Society, London, Special Publications* **156**, 475-515 (1999).
107. A. M. Álvarez-Valero *et al.*, *Bulletin* **126**, 1614-1624 (2014).
108. M. Alavi, *Tectonophysics* **229**, 211-238 (1994).
109. W. Xiao, B. Windley, J. Hao, J. Li, *Journal of the Geological Society* **159**, 517-528 (2002).
110. M. Schwab *et al.*, *Tectonics* **23**, (2004).
111. E. Enkelmann *et al.*, *Tectonics* **26**, (2007).
112. T. N. Yang, Z. Q. Hou, Y. Wang, H. R. Zhang, Z. L. Wang, *Tectonics* **31**, (2012).
113. K.-J. Zhang, Y.-X. Zhang, X.-C. Tang, B. Xia, *Earth-Science Reviews* **114**, 236-249 (2012).
114. Q.-G. Zhai, B.-M. Jahn, R.-Y. Zhang, J. Wang, L. Su, *Journal of Asian Earth Sciences* **42**, 1356-1370 (2011).
115. R. A. Beck *et al.*, *Nature* **373**, 55 (1995).
116. P. Bouilhol, O. Jagoutz, J. M. Hanchar, F. O. Dudas, *Earth and Planetary Science Letters* **366**, 163-175 (2013).
117. R. Hébert *et al.*, *Gondwana Research* **22**, 377-397 (2012).
118. O. Jagoutz, L. Royden, A. F. Holt, T. W. Becker, *Nature Geoscience* **8**, 475 (2015).
119. I. Metcalfe, *Journal of Asian Earth Sciences* **66**, 1-33 (2013).
120. J.-W. Zi *et al.*, *Lithos* **144**, 145-160 (2012).
121. P. Jian *et al.*, *Lithos* **113**, 767-784 (2009).
122. B. C. Burchfiel, Z. Chen, *Tectonics of the Southeastern Tibetan Plateau and its Adjacent Foreland*. (Geological Society of America, 2012), vol. 210.
123. R. Pedersen, M. Searle, A. Carter, P. Bandopadhyay, *Journal of the Geological Society* **167**, 1105-1112 (2010).
124. R. Allen *et al.*, **436**, 223 (2008).
125. H. Zwart, *Medd. Dan. Geol. Foren* **17**, 504-516 (1967).
126. U. Kroner, R. Romer, *Gondwana Research* **24**, 298-329 (2013).
127. A. J. Hartley, J. Otava, *Journal of the Geological Society* **158**, 137-150 (2001).
128. R. Gayer, J. Jones, *Proceedings of the Ussher Society* **7**, 177-179 (1989).
129. A. Schäfer, *Geologische Rundschau* **78**, 499-524 (1989).
130. M. Narkiewicz, *Geological Quarterly* **51**, 231-256 (2010).
131. E. Garzanti, M. Gaetani, *Sedimentary Geology* **151**, 67-87 (2002).
132. H. S. Moghadam, R. J. Stern, *Journal of Asian Earth Sciences* **91**, 19-38 (2014).

133. C. R. van Staal, S. M. Barr, J. Percival, *Tectonic styles in Canada: the LITHOPROBE perspective. Edited by JA Percival, FA Cook, and RM Clowes. Geological Association of Canada, Special Paper* **49**, (2012).
134. C. A. Ver Straeten, *From Rodinia to Pangea: The Lithotectonic Record of the Appalachian Region. Geological Society of America Memoir* **206**, 251-282 (2010).
135. A. Piqué, J. W. Skehan, *Tectonics* **11**, 392-404 (1992).
136. R. D. Nance *et al.*, **17**, 194-222 (2010).
137. M. Villeneuve, *Journal of African Earth Sciences* **43**, 166-195 (2005).
138. A. Pique, A. Michard, *American Journal of science* **289**, 286-330 (1989).
139. R. D. Dallmeyer, J. E. Wright, D. T. Secor Jr., A. Snoke, **97**, 1329-1344 (1986).
140. J. D. Gleason, P. J. Patchett, W. R. Dickinson, J. Ruiz, **107**, 1192-1210 (1995).
141. K. C. Misra, F. B. Keller, *American Journal of Science* **278**, 389-418 (1978).
142. S. Hollis *et al.*, *Journal of the Geological Society* **170**, 861-876 (2013).
143. R. Pedersen, H. Furnes, *Journal of Geodynamics* **13**, 183-203 (1991).
144. D. G. Gee, H. Fossen, N. Henriksen, A. K. Higgins, *Episodes* **31**, 44-51 (2008).
145. W. C. McClelland, S. J. Malone, W. von Gosen, K. Piepjohn, A. Läufer, *Zeitschrift der deutschen Gesellschaft fuer Geowissenschaften* **163**, 251-259 (2012).
146. H. P. Trettin, in *Geology of the Innuitian Orogen and Arctic Platform of Canada and Greenland*, H. P. Trettin, Ed. (Geological Survey of Canada, 1991), vol. 3, pp. 241-259.
147. H. Trettin, R. Parrish, J. Roddick, *Geological Survey of Canada Paper 92-2*, 3-30 (1992).
148. T. Pharaoh, *Tectonophysics* **314**, 17-41 (1999).
149. B. F. Windley, D. Alexeiev, W. Xiao, A. Kroener, G. Badarch, *Journal of the Geological Society of London* **164**, 31-47 (2007).
150. W. Xiao *et al.*, *Annual Review of Earth and Planetary Sciences* **43**, 477-507 (2015).
151. U. Bold, J. L. Crowley, E. F. Smith, O. Sambuu, F. A. Macdonald, *Lithosphere* **8**, 729-750 (2016).
152. E. F. Smith, F. A. Macdonald, T. A. Petach, U. Bold, D. P. Schrag, *Geological Society of America Bulletin* **128**, 442-468 (2015).
153. N. Dobretsov, M. Buslov, *Russian Geology and Geophysics* **48**, 71-82 (2007).
154. T. Cherkasova, A. Chernishov, Y. Goltsova, T. Timkin, R. Abramova, in *IOP Conference Series: Earth and Environmental Science*. (IOP Publishing, 2015), vol. 27, pp. 012002.
155. I. K. Kozakov *et al.*, *Geotectonics* **46**, 16-36 (2012).
156. C. Buchan, D. Cunningham, B. Windley, D. Tomurhuu, *Journal of the Geological Society of London* **158**, 445-460 (2001).
157. R. Van der Voo, D. J. van Hinsbergen, M. Domeier, W. Spakman, T. H. Torsvik, *Geological Society of America Special Papers* **513**, 589-606 (2015).
158. T. Donskaya, D. Gladkochub, A. Mazukabzov, A. Ivanov, *Journal of Asian Earth Sciences* **62**, 79-97 (2013).
159. A. Kröner *et al.*, *American Journal of Science* **310**, 523-574 (2010).
160. H. Liu, I. D. Somerville, C. Lin, S. Zuo, *Geological Journal* **51**, 627-651 (2016).
161. J.-X. Zhang *et al.*, *Tectonophysics* **570**, 78-101 (2012).
162. S. Song, Y. Niu, L. Su, X. Xia, *Gondwana Research* **23**, 1378-1401 (2013).
163. B. R. Hacker, L. Ratschbacher, J. Liou, *Geological Society, London, Special Publications* **226**, 157-175 (2004).
164. D. Cluzel, *Journal of Southeast Asian Earth Sciences* **7**, 195-209 (1992).
165. A. Ishiwatari, T. Tsujimori, *Island Arc* **12**, 190-206 (2003).

166. B.-F. Han *et al.*, *Bulletin* **122**, 627-640 (2010).
167. B. Wang *et al.*, **497**, 85-104 (2011).
168. F. Choulet *et al.*, **312**, 1098-1145 (2012).
169. D. Alexeiev *et al.*, **42**, 805-820 (2011).
170. A. Kröner *et al.*, **21**, 901-927 (2012).
171. D. Alexeiev *et al.*, **39**, 261-291 (2016).
172. D. Brown *et al.*, *Earth-Science Reviews* **79**, 261-287 (2006).
173. L. Zonenshain *et al.*, *Tectonophysics* **109**, 95-135 (1984).
174. P. Spadea, M. D'Antonio, *Island Arc* **15**, 7-25 (2006).
175. J. Proust, B. Chuvashov, E. Vennin, T. Boisseau, *Journal of Sedimentary Research* **68**, (1998).
176. A. J. Newell, V. P. Tverdokhlebov, M. J. Benton, *Sedimentary Geology* **127**, 11-29 (1999).
177. P. A. Cawood, *Earth-Science Reviews* **69**, 249-279 (2005).
178. R. Glen, *Geological Society of London, Special Publication* **246**, 23 (2005).
179. C. V. Spaggiari, D. R. Gray, D. A. Foster, *Geological Society, London, Special Publications* **218**, 517-539 (2003).
180. G. Rosenbaum, *Episodes* **35**, 187-194 (2012).
181. V. A. Ramos, M. Escayola, D. I. Mutti, G. I. Vujovich, *Geological Society of America, Special Papers*, 331-350 (2000).
182. C. Casquet *et al.*, *Earth-Science Reviews*, (2017).
183. M. P. Escayola, M. M. Pimentel, R. Armstrong, *Geology* **35**, 495-498 (2007).
184. R. E. Ernst, N. Youbi, *Palaeogeography, Palaeoclimatology, Palaeoecology* **478**, 30-52 (2017).
185. K. P. Norton, P. Molnar, F. J. G. Schlunegger, **204**, 510-517 (2014).
186. Y. Goddéris *et al.*, **42**, 151-162 (2017).
187. L. Johansson, S. Zahirovic, R. D. Müller, *Geophysical Research Letters*, (2018).
188. G. J. P. T. Hadley, **39**, 58-62 (1735).
189. A. Donohoe, A. J. C. E. P. Voigt, Mechanisms, 115-137 (2017).
190. E. Kalnay *et al.*, *Bulletin of the American Meteorological Society* **77**, 437-472 (1996).
191. D. G. Van Der Meer *et al.*, *Proceedings of the National Academy of Sciences* **111**, 4380-4385 (2014).
192. I. P. Montanez, *Geochimica et Cosmochimica Acta* **101**, 57-75 (2013).
193. J. Higgins *et al.*, *Geochimica et Cosmochimica Acta* **220**, 512-534 (2018).
194. D. L. Royer, Y. Donnadieu, J. Park, J. Kowalczyk, Y. Goddéris, *American Journal of Science* **314**, 1259-1283 (2014).
195. T. J. Crowley, *Oxford Monographs on Geology and Geophysics* **39**, 3-20 (1998).
196. R. A. Berner, Z. Kothavala, *American Journal of Science* **301**, 182-204 (2001).
197. L. Frakes, J. Francis, *Nature* **333**, 547 (1988).
198. T. H. Torsvik, L. R. M. Cocks, *Gondwana Research* **24**, 999-1030 (2013).
199. M. R. Saltzman, S. A. Young, *Geology* **33**, 109-112 (2005).
200. M. Hambrey, *Palaeogeography, Palaeoclimatology, Palaeoecology* **51**, 273-289 (1985).
201. E. Díaz-Martínez, Y. Grahn, *Palaeogeography, Palaeoclimatology, Palaeoecology* **245**, 62-81 (2007).
202. P. Isaacson *et al.*, *Palaeogeography, Palaeoclimatology, Palaeoecology* **268**, 126-142 (2008).

203. P. Fuentes, J. Díaz-Alvarado, C. Fernández, M. Díaz-Azpiroz, N. Rodríguez, *Journal of South American Earth Sciences* **67**, 40-56 (2016).
204. D. K. Brezinski, C. B. Cecil, V. W. Skema, R. Stamm, *Palaeogeography, Palaeoclimatology, Palaeoecology* **268**, 143-151 (2008).
205. J. t. Veevers, C. M. Powell, *Geological Society of America Bulletin* **98**, 475-487 (1987).
206. I. P. Montañez, C. J. Poulsen, *Annual Review of Earth and Planetary Sciences* **41**, 629-656 (2013).
207. C. R. Fielding, T. D. Frank, J. L. Isbell, *Resolving the Late Paleozoic ice age in time and space*. (Geological Society of America, 2008), vol. 441.
208. L. Frakes, N. Alley, M. J. I. G. R. Deynoux, **37**, 567-583 (1995).
209. J. Zachos, M. Pagani, L. Sloan, E. Thomas, K. Billups, *Science* **292**, 686-693 (2001).
210. B. De Boer, R. Van de Wal, R. Bintanja, L. Lourens, E. Tuenter, *Annals of Glaciology* **51**, 23-33 (2010).
211. L. C. Ivany, S. Van Simaeys, E. W. Domack, S. D. Samson, *Geology* **34**, 377-380 (2006).
212. A. L. Troedson, J. B. Riding, *Journal of Sedimentary Research* **72**, 510-523 (2002).
213. R. Dingle, M. Lavelle, *Journal of the Geological Society* **155**, 433-437 (1998).
214. J. Ehlers, P. L. Gibbard, *Quaternary International* **164**, 6-20 (2007).
215. H. Von Storch, in *Analysis of Climate Variability*. (Springer, 1999), pp. 11-26.
216. V. Puchkov, R. E. Ernst, M. A. Hamilton, U. Söderlund, N. Sergeeva, *GFF* **138**, 6-16 (2016).
217. D. V. Kent, G. Muttoni, *Proceedings of the National Academy of Sciences* **105**, 16065-16070 (2008).
218. C.-T. A. Lee, J. S. Lackey, *Elements* **11**, 125-130 (2015).